Magnetic-field Induced Pair Density Wave State in the Cuprate Vortex Halo

S. D. Edkins[1,2,3], A. Kostin[1], K. Fujita[1,4], A. P. Mackenzie[3,5], H. Eisaki[6], S. Uchida[7], Subir Sachdev[8], M. J. Lawler[1,9], E-A. Kim[1], J.C. Séamus Davis[1,4,10,11], and M. H. Hamidian[1,8]

1. *LASSP, Department of Physics, Cornell University, Ithaca, NY 14853, USA.*
2. *Department of Applied Physics, Stanford University, Stanford, CA 94305, USA*
3. *School of Physics and Astron., University of St. Andrews, Fife KY16 9SS, Scotland.*
4. *Condensed Matter Physics Department, Brookhaven National Lab., Upton NY, USA.*
5. *Max-Planck Institute for Chemical Physics of Solids, D-01187 Dresden, Germany.*
6. *Inst. of Advanced Industrial Science and Tech., Tsukuba, Ibaraki 305-8568, Japan.*
7. *Department of Physics, University of Tokyo, Bunkyo-ku, Tokyo 113-0033, Japan.*
8. *Department of Physics, Harvard University, Cambridge, MA 02138, USA*
9. *Dept. of Physics and Astronomy, Binghamton University, Binghamton, NY 13902, USA.*
10. *Department of Physics, University College Cork, Cork T12R5C, Ireland.*
11. *Clarendon Laboratory, Oxford University, Oxford, OX1 3PU, UK.*

High magnetic fields suppress cuprate superconductivity to reveal an unusual density wave (DW) state coexisting with unexplained quantum oscillations. Although routinely labeled a charge density wave (CDW), this DW state could actually be an electron-pair density wave (PDW). To search for evidence of a field-induced PDW, we visualize modulations in the density of electronic states $N(\boldsymbol{r})$ within the halo surrounding $Bi_2Sr_2CaCu_2O_8$ vortex cores. Numerous phenomena predicted for a field-induced PDW are detected, including two sets of particle-hole symmetric $N(\boldsymbol{r})$ modulations with wavevectors $\boldsymbol{Q_P}$ and $2\boldsymbol{Q_P}$, with the latter decaying twice as rapidly from the core as the former. These data imply that the primary field-induced state in underdoped superconducting cuprates is a PDW, with approximately eight CuO_2 unit-cell periodicity and coexisting with its secondary CDWs.

1 Theory predicts that Cooper-pairs with finite center-of-mass momentum $\boldsymbol{p} = \hbar\boldsymbol{Q}_P$ should form a state in which the density of pairs modulates spatially at wavevector $\boldsymbol{Q_P}$ *(1,2)*. In the phase diagram of underdoped cuprates, such a 'pair density wave' (PDW) state (*3-5*), generated by strong local electron-electron interactions *(6-11)*, is anticipated to be another principal state along with uniform superconductivity. Numerous experimental observations may be understood in that context. For example, although intra-planar superconductivity appears in $La_{2-x}Ba_xCuO_4$ at relatively high temperatures, inter-planar superconductivity is strongly frustrated (*12*), consistent with the existence of orthogonal unidirectional PDW states in each sequential CuO_2 plane (*3,13,14*). Moreover, the measured momentum-space electronic structure of the cuprate pseudogap phase is consistent with predictions based on a biaxial PDW *(4)*. Reported breaking of time-reversal symmetry could be caused by a PDW with inversion breaking (*15-18).* The field-induced momentum-space reconstruction and quantum oscillation phenomenology are potentially the consequences of a PDW state (*19-21*) although this view is not universal (*22*). At highest fields, strong diamagnetism in torque magnetometry (*23*) and supercurrents in DC transport might also be understood as due to a field-induced PDW state. Most recently, scanned Josephson tunneling microscopy allows direct visualization of cuprate pair density modulations (*24*). Taken together, these studies indicate that a fundamental PDW state may exist in underdoped cuprates, with the most common model invoked being an eight unit-cell ($8a_0$) periodic modulation of the electron-pair condensate.

2 Such a PDW state clearly does not predominate at low temperature in zero magnetic field where global *d*-wave superconductivity is robust. However, suppression of the superconductivity by high magnetic fields generates a peculiar DW state (*25-32*) along with exotic quantum oscillation phenomenology (*33,34*). For type-II superconductors in general, application of a magnetic field generates quantized vortices. At the vortices of a conventional *d*-wave superconductor, the four zeros in the energy-gap should generate a slowly decaying, star-shaped, zero-energy resonance oriented along the nodal $(\pm 1, \pm 1)$ directions. For cuprates, however, strong $N(\boldsymbol{r}, E)$ modulations oriented along (1,0); (0,1) directions have long been observed in the 'halo' region surrounding the cuprate vortex core (*35-38).* Many theories hypothesize that this phenomenon is a field-induced DW (*5,39-43)* and some that is not a conventional CDW but a PDW (*4,5,22,43*). This is a fundamental distinction because the PDW and CDW are extremely different states in terms of their broken symmetries and many-body wavefunctions. Thus, to determine whether the primary DW state induced by magnetic field in superconducting cuprates is a PDW has recently become an urgent research challenge.

3 To search for evidence of such a state, we study the field-induced modulations of the density of electronic states $N(\boldsymbol{r}, E)$ within the halo surrounding quantized vortex cores (*35-38*). Any periodic modulations of electronic structure can be described by $A(\boldsymbol{r}) = AF(\theta)\cos(\boldsymbol{Q}\cdot\boldsymbol{r} + \phi_0)$, where $A(\boldsymbol{r})$ represents the modulating electronic degree of freedom with amplitude A, $\boldsymbol{Q}$ is the wavevector, and $F(\theta)$ is the modulation form factor defined in terms of the angle θ from the (1,0) axis. An *s*-symmetry form factor $F_s(\theta)$ is even under 90° rotations whereas a *d*-wave form factor is $F_d(\theta)$ is odd. Following Ref. 5, the order parameters we consider are those of homogenous *d*-wave superconductivity $\Delta(\boldsymbol{r}) = F_{SC}\Delta_{SC}$ with $F_{SC} = F_d$, and that of a pair density wave $\Delta_{PD}(\boldsymbol{r}) = F_P\Delta_P^Q\left[e^{i\boldsymbol{Q_P}\cdot\boldsymbol{r}} + e^{-i\boldsymbol{Q_P}\cdot\boldsymbol{r}}\right]$ with wavevector $\boldsymbol{Q_P}$ and either an F_s or F_d type of form factor (Section 1 Ref. 44). A field-induced PDW may be identified from Ginzburg-Landau (GL) analysis (*5,22,43*) of the interactions between these two OP within vortex halos – regions of suppressed but non-zero superconductivity that surround vortex cores (Fig. 1A). Given a generic GL free energy density of the form

$$\mathcal{F}_{A-SC} = \mathcal{F}(\Delta_{SC}) + \mathcal{F}(\Delta_A) + u_1|\Delta_A|^2|\Delta_{SC}|^2 \qquad (1)$$

where (Δ_{SC}) and $\mathcal{F}(\Delta_A)$ are the free energy densities of a superconductor and of an alternative repulsively-coupled (u_1>0) state Δ_A, the observation of coexistence of Δ_A with Δ_{SC} within the vortex halo (Section 2, Ref. 44) means that the two ordered states are almost energetically degenerate (*39*). Such a near degeneracy occurs naturally between a superconductor Δ_{SC} and a PDW Δ_P^Q, that are made up of the same electron-pairs. In this case, allowed $N(\boldsymbol{r})$ modulations generated by interactions between Δ_{SC} and Δ_A can be found from products of these order parameters that transform as density-like quantities. For example, the product of PDW and uniform SC order parameters

$$A_{\boldsymbol{Q_P}} \propto \Delta_P^Q\Delta_{SC}^* \Rightarrow N(\boldsymbol{r}) \propto \cos(\boldsymbol{Q_P}.\boldsymbol{r}) \qquad (2)$$

results in $N(\boldsymbol{r})$ modulations at the PDW wavevector $\boldsymbol{Q_P}$. The product of a robust PDW with itself

$$A_{2\boldsymbol{Q_P}} \propto \Delta_P^Q\Delta_P^{-Q*} \Rightarrow N(\boldsymbol{r}) \propto \cos(2\boldsymbol{Q_P}.\boldsymbol{r}) \qquad (3)$$

produces $N(\boldsymbol{r})$ modulations occurring at $\boldsymbol{2Q_P}$. Thus, a key signature of a field-induced PDW with wavevector $\boldsymbol{Q_P}$ in cuprate vortex halos (Fig. 1A), would be coexistence of two sets of $N(\boldsymbol{r})$ modulations at $\boldsymbol{Q_P}$ and at $\boldsymbol{2Q_P}$ within each halo (*5,22,43*) (Fig. 1B).

4 Within Ginzburg-Landau (GL) theory, significant further information can be extracted from measured rates of decay of the induced $N(\boldsymbol{r})$ modulations away from the vortex center, and from the form factors of these modulations within the vortex halo. For a field-induced PDW, the $N(\boldsymbol{r},E)$ modulations at $\boldsymbol{2Q_P}$ should decay with distance from the core at twice the rate as those at $\boldsymbol{Q_P}$. This is because, if $\Delta_P^Q = \Delta_P^Q(|\boldsymbol{r}|=0)e^{-|r|/\xi}$, then $\Delta_P^Q\Delta_P^{-Q*}$ decays with $|\boldsymbol{r}|$ at twice the rate of $\Delta_P^Q\Delta_{SC}^*$ (Fig. 1B). Current theory (*22*,*43*) indicates that, if the $N(\boldsymbol{r},E)$ modulations at $\boldsymbol{Q_P}$ caused by $\Delta_P^Q\Delta_{SC}^*$ exhibit *s*-symmetry form factor (F_s) this implies the PDW order parameter Δ_P^Q contains components with *d*-symmetry form factor (F_d), and vice versa (Section 2, Ref. 44). These studies (*22*,*43*) sustain the original Ginzburg-Landau approach (*5*) by showing that an $8a_0$ PDW stabilized in the halo of a *d*-wave vortex core does indeed generate both an $8a_0$ and a $4a_0$ periodic charge modulation therein. Overall, because a *d*-symmetry form factor PDW is typically predicted for cuprates (*6-11*), its signature within a vortex halo should be two sets of $N(\boldsymbol{r})$ modulations occurring at $\boldsymbol{Q_P}$ and $\boldsymbol{2Q_P}$, both with *s*-symmetry form factor components, and with the amplitude of the $\boldsymbol{2Q_P}$ modulation decaying twice as rapidly as that at $\boldsymbol{Q_P}$.

5 To explore these predictions, we image scanning tunneling microscope (STM) tip-sample differential tunneling conductance $dI/dV\,(\boldsymbol{r},V) \equiv g\,(\boldsymbol{r},E)$, versus bias voltage *V=E/e* and location $\boldsymbol{r}$ with sub-unit-cell spatial resolution; no scanned Josephson tunneling microscopy (*24*) is involved. We measure slightly underdoped $Bi_2Sr_2CaCu_2O_8$ samples (T_c~88K; p~17%)) at T=2K. The $N(\boldsymbol{r},E)$ is first measured at zero field and then at magnetic field B=8.25T, in the identical field of view (FOV) using an identical STM tip (*35*). The former is subtracted from the latter to yield the field-induced changes $\delta g(\boldsymbol{r},E,B) = g(\boldsymbol{r},E,B) - g(\boldsymbol{r},E,0)$, which are related to the field-induced perturbation to the density of states as $\delta N(\boldsymbol{r},E,B) \propto \delta g(\boldsymbol{r},E,B)$. This step ensures that the phenomena studied hereafter are only those induced by the magnetic field, with all signatures of the ubiquitous *d*-symmetry form factor DW observed at *B*=0 (Ref. 45) having been subtracted. Compared to our prior vortex halo studies (*35*), we enhanced the $\boldsymbol{r}$-space resolution using smaller pixels and the $\boldsymbol{q}$-space resolution by using larger FOV (58nmX58nm), increased the number of vortices per image, used distortion-corrected sublattice-phase-resolved imaging (*45*), and measured in a far wider energy range 0<|E|<80meV (Section 3, Ref. 44).

6 The location of every vortex halo in $\delta g(\boldsymbol{r},E,B)$ images is next identified by using two well-known phenomena: (i) suppression of the superconducting coherence peaks at the vortex symmetry point (Fig. 2B) and, (ii) appearance of low-energy periodic conductance modulations (*35-38*) surrounding this point. Figure 2B shows a typical symmetry-point spectrum of the superconducting vortex where maximum suppression of the single-particle coherence peaks occurs; these peaks recover very rapidly as a function of radius, so that robust *d*-wave superconductivity signified by full coherence peaks has recovered within a radius of ~1nm (Section 4, Ref. 44). At E=12meV, the typical 'halo' of conductance modulations we detect surrounding each vortex symmetry-point (Fig. 2C) is in excellent agreement with previous studies of modulations of low-energy quasiparticles with $\boldsymbol{q} \approx (\pm 1/4,0);(0,\pm 1/4)2\pi/a_0$ within the $Bi_2Sr_2CaCu_2O_{8-x}$ vortex halo (*35-38*). Here we focus on a different energy range 25<|E|<50 meV because analysis of our $\delta g(\boldsymbol{r},E)$ data reveals major changes in this range. In Fig. 3A we show measured $\delta g(\boldsymbol{r},30\text{meV})$ containing the modulations detected in the halo of each vortex core. Fourier analysis of this $\delta g(\boldsymbol{r},30\text{meV})$ yields $|\widetilde{\delta g}(\boldsymbol{q},30\text{meV})|$ (Fig. 3B) reveals a set of sharp peaks at $\boldsymbol{q}=[\boldsymbol{Q_P^x};\boldsymbol{Q_P^y}] \approx [(\pm 1/8,0);(0,\pm 1/8)]\ 2\pi/a_0$ which we label $\boldsymbol{Q_P}$ for reasons explained below. Similarly, there is a second set of weaker modulations in $\widetilde{\delta g}(\boldsymbol{q},30\text{meV})$ at $\boldsymbol{q} \approx [(\pm 1/4,0);(0,\pm 1/4)]\ 2\pi/a_0$ which we label $2\boldsymbol{Q_P}$. The $\boldsymbol{r}$-space amplitude-envelopes of the $\boldsymbol{Q_P}$ and $2\boldsymbol{Q_P}$ modulations (Figs. 3C and D) reveal how these field-induced phenomena are confined to the vortex halo regions only. Averaged over all vortices, the measured amplitude $\left|\widetilde{\delta g}(\boldsymbol{q},30\text{meV})\right|$ plotted along (1,0) in Fig. 3E discernibly discriminates the $\boldsymbol{Q_P}$ from the $\boldsymbol{2Q_P}$ modulation peaks. Thus, we discover strong, field-induced modulations of $N(\boldsymbol{r},E)$ with period approximately $8a_0$ coexisting with weaker modulations of period approximately $4a_0$, along both the (1,0);(0,1) directions within every vortex halo. These particle-hole symmetric phenomena exist within the energy range 25<|E|<45 meV (Section 5, Ref. 44).

7 To evaluate form factor symmetry for these field-induced modulations (Section 6, Ref. 44), we separate each such $\delta g(\boldsymbol{r}, E)$ image into three sublattice images (*46*): $Cu(\boldsymbol{r}, E)$, containing only the measured values of $\delta g(\boldsymbol{r}, E)$ at copper sites and $O_x(\boldsymbol{r}, E)$ and $O_y(\boldsymbol{r}, E)$, containing only those at the x/y-axis oxygen sites. All of the form factors discussed here refer to modulations in $\delta g(\boldsymbol{r}, E, B)$ and are not necessarily those of the order parameter of the field–induced state that generates them. Complex-valued Fourier transforms of the $O_x(\boldsymbol{r}, E)$ and $O_y(\boldsymbol{r}, E)$ sublattice images, yield $\tilde{O}_x(\boldsymbol{q}, E)$; $\tilde{O}_y(\boldsymbol{q}, E)$. Then, modulations at any $\boldsymbol{Q}$ having d-symmetry form factor F_d generate a peak in $\tilde{D}^{\delta g}(\boldsymbol{q}, E) \equiv \tilde{O}_x(\boldsymbol{q}, E) - \tilde{O}_y(\boldsymbol{q}, E)$ at $\boldsymbol{Q}$, whereas those with s-symmetry form factor F_s generate a peak in $\tilde{S}^{\delta g}(\boldsymbol{q}, E) \equiv (\tilde{O}_x(\boldsymbol{q}, E) + \tilde{O}_y(\boldsymbol{q}, E)) + \widetilde{Cu}(\boldsymbol{q}, E)$ at $\boldsymbol{Q}$. When the data in Figs. 3A,B are analyzed in this way using measured $\tilde{S}^{\delta g}(\boldsymbol{q}, 30\text{meV})$, the field-induced $\delta g(\boldsymbol{r}, E)$-modulations occurring at $\boldsymbol{q} \approx (\pm Q_P, 0); (0, \pm Q_P)$ and $\boldsymbol{q} \approx (\pm 2Q_P, 0); (0, \pm 2Q_P)$ all exhibit s-symmetry form factors (Fig. 3E). However, the measured $\tilde{D}^{\delta g}(\boldsymbol{q}, 30\text{meV})$ in Figs. 3F and G also reveals that weaker d-symmetry $\delta g(\boldsymbol{r}, E)$-modulations occur at $\boldsymbol{q} \approx (0, \pm Q_P)$ and $\boldsymbol{q} \approx (0, \pm 2Q_P)$. They too are confined to the vortex halo because the $\boldsymbol{r}$-space amplitude-envelope of the $\boldsymbol{2Q_P}$-modulations in $\tilde{D}^{\delta g}(\boldsymbol{q}, 30\text{meV})$ is concentrated there.

8 Figures 4A and B show the overall measured amplitudes of $|\widetilde{\delta g}(\boldsymbol{q}, 30\text{meV})|$ derived from $\delta g(\boldsymbol{r}, 30\text{meV})$ in Fig. 3A, plotted along the (1,0) and (0,1) directions of the CuO_2 plane. Figures. 4C and D show equivalent cuts of $\left|\widetilde{\delta g}(\boldsymbol{q}, -30\text{meV})\right|$ derived from $\delta g(\boldsymbol{r}, -30\text{meV})$ data. The four maxima at $|\boldsymbol{q}| \approx 1/8$, $|\boldsymbol{q}| \approx 1/4$, $|\boldsymbol{q}| \approx 3/4$ and $|\boldsymbol{q}| \approx 7/8$ associated with field induced modulations occur in Fig. 4A-D. The measured form factor of each set of modulations is identified by color code, red being s-symmetry and blue d-symmetry. Although modulations at $|\boldsymbol{q}| \approx 7/8$, $|\boldsymbol{q}| \approx 3/4$ (blue Fig. 4A-D) appear subdominant, they do merit comment. First, they are not inconsistent with an admixture of s-symmetry and d-symmetry components in the PDW order parameter. However, these modulations may also represent a field-induced version of the unidirectional d-symmetry form factor N($\boldsymbol{r}$,E) modulation observed in zero field (*45*).

9 But the predominant phenomena detected are the two sets of *s*-symmetry form factor modulations at $|\boldsymbol{Q_P}| \approx 1/8$, $|\boldsymbol{2Q_P}| \approx 1/4$ (red Fig. 4A-D). Moreover, after subtraction of a smooth background, the widths δq of all $|\boldsymbol{Q_P}| \approx 1/8$ peaks are close to half of the $|\boldsymbol{2Q_P}| \approx 1/4$ peaks, as determined quantitatively by fitting as shown in Figs. 4A-D. Averaged over the two directions (1,0) and (0,1) and energies $E = \pm 30$meV, we find that $\delta(2Q_P) = (1.8 \pm 0.2)\,\delta(Q_P)$ as expected for a field-induced PDW (*5,22,43*) (Fig. 1). As additional evidence of a PDW, we search for energy gap modulations in measured $\Delta(\boldsymbol{r}) = \Delta_{SC} + \Delta_P cos(\boldsymbol{Q_P} \cdot \boldsymbol{r})$. Generally, in superconductivity studies, the empirical $\Delta(\boldsymbol{r})$ is defined as half the energy separation of the coherence peaks in $N(\boldsymbol{r}, E)$ (horizontal arrow in Fig. 2A), so that field-induced changes to $\Delta(\boldsymbol{r})$ would here be defined as $\delta\Delta(\boldsymbol{r}) = \Delta(\boldsymbol{r}, 8.25T) - \Delta(\boldsymbol{r}, 0)$) (Section 7, Ref. 44). When measured, this $\delta\Delta(\boldsymbol{r})$ yields a Fourier transform $\widetilde{\delta\Delta}(\boldsymbol{q})$ as shown in Fig. 4E. This exhibits evidence for a field-induced energy-gap modulation at $\boldsymbol{Q_P}$ and not at $\boldsymbol{2Q_P}$, as would be expected specifically for a primary field-induced PDW at $\boldsymbol{Q_P}$.

10 Taken together, the results shown in Figures 3 and 4 indicate that, in $Bi_2Sr_2CaCu_2O_8$, a field-induced pair density wave state emerges within the halo region surrounding each quantized vortex core. The principal experimental signatures are two sets of $N(\boldsymbol{r})$ modulations occurring at $\boldsymbol{Q_P}$ and $\boldsymbol{2Q_P}$, both being particle-hole symmetric, both exhibiting principal amplitude with *s*-symmetry form factor, with the amplitude of $\boldsymbol{2Q_P}$ modulations decaying twice as rapidly as that of $\boldsymbol{Q_P}$, and with an apparently bi-directional structure as shown schematically in Fig. 4F (see Section 8 of Ref. 44). These phenomena occur in an energy range 25<|E|<45meV, as might be expected theoretically for an $8a_0$ periodic PDW with energy gap magnitude Δ_P^Q occurring within that range. Several significant implications stem from these observations. First and foremost, the primary state induced by high magnetic fields in the superconducting phase of cuprates is inferred to be a PDW with wavevector $\boldsymbol{Q_P}$, accompanied by secondary charge modulations at $\boldsymbol{Q_P}$ and $\boldsymbol{2Q_P}$. Second, the $8a_0$ periodicity points towards a strong-correlation driven microscopic mechanism for the PDW (*6-11*), in which case the form factor is generally predicted to have a *d*-symmetry (Fig. 4F). Third, because the PDW is generated by increasing magnetic field, our data imply that the high-field state of cuprates might itself be a PDW state (*4*) and, if so, it is likely phase fluctuating and intertwined with additional CDW components. Finally, putting all such conjectures aside, we emphasize that the experimental observations reported in Figs. 3,4 are in good, detailed and quantitative agreement with theoretical models *(5,22,43,44*) for a primary PDW with wavevector $\boldsymbol{Q_P}$ induced within the cuprate vortex halo, that generates secondary CDWs at $\boldsymbol{Q_P}$ and $\boldsymbol{2Q_P}$.

References and Notes

1. P. Fulde, R. A. Ferrell, Superconductivity in a Strong Spin-Exchange Field. *Physical Review* **135**, A550–A563 (1964).

2. A. I. Larkin, Y. N. Ovchinnikov, Inhomogeneous state of superconductors. *Sov. Phys. JETP* **20**, 762– 769 (1964).

3. E. Berg, E. Fradkin, E. A. Kim, S. A. Kivelson, V. Oganesyan, J. M. Tranquada, S. C. Zhang, Dynamical layer decoupling in a stripe-ordered high-T_c superconductor. *Physical Review Letters* **99**, 127003 (2007).

4. P. A. Lee, Amperean pairing and the pseudogap phase of cuprate superconductors. *Physical Review X* **4**, 1–13 (2014).

5. D. F. Agterberg, J. Garaud, Checkerboard order in vortex cores from pair-density-wave superconductivity. *Physical Review B* 104512 (2015).

6. A. Himeda, T. Kato, M. Ogata, Stripe states with spatially oscillating d-wave superconductivity in the two-dimensional *t-t'-J* model. *Physical Review Letters* **88**, 117001 (2002).

7. M. Raczkowski, M. Capello, D. Poilblanc, R. Fr´esard, A. M. Ole ´s, Unidirectional d-wave superconducting domains in the two-dimensional *t–J* model. Physical Review B **76**, 140505 (2007).

8. K.-Y. Yang, W. Q. Chen, T. M. Rice, M. Sigrist, F.-C. Zhang, Nature of stripes in the generalized *t-J* model applied to the cuprate superconductors. *New Journal of Physics* **11**, 055053 (2009).

9. F. Loder, A. P. Kampf, T. Kopp, Superconducting state with a finite-momentum pairing mechanism in zero external magnetic field. *Physical Review B* **81**, 020511(R) (2010).

10. P. Corboz, T. M. Rice, M. Troyer, Competing states in the t-J model: Uniform d-wave state versus stripe state. *Physical Review Letters* **113**, 046402 (2014).

11. R.-G. Cai, L. Li, Y.-Q. Wang, J. Zaanen, Intertwined Order and Holography: The Case of Parity Breaking Pair Density Waves. *Phys. Rev. Lett.* **119**, 181601 (2017).

12. Q. Li, M. H¨ucker, G. D. Gu, A. M. Tsvelik, J. M. Tranquada, Two-dimensional superconducting fluctuations in stripe-ordered $La_{1.875}Ba0_{.125}CuO_4$. *Physical Review Letters* **99**, 067001 (2007).

13. E. Berg, E. Fradkin, S. A. Kivelson, Charge-4e superconductivity from pair density wave order in certain high temperature superconductors. *Nature Physics* **5**, 830–833 (2009).

14. E. Berg, E. Fradkin, S. A. Kivelson, J. M. Tranquada, Striped superconductors: how spin, charge and superconducting orders intertwine in the cuprates. *New Journal of Physics* **11**, 115004 (2009).

15. C. P´epin, V. S. De Carvalho, T. Kloss, X. Montiel, Pseudogap, charge order, and pairing density wave at the hot spots in cuprate superconductors. *Physical Review B* **90**, 195207 (2014).

16. H. Freire, V. S. de Carvalho, C. P´epin, Renormalization group analysis of the pair-density-wave and charge order within the fermionic hot-spot model for cuprate superconductors. *Physical Review B* **92**, 045132 (2015).

17. Y. Wang, D. F. Agterberg, A. Chubukov, Coexistence of charge-density-wave and pair-density-wave orders in underdoped cuprates. *Physical Review Letters* **114**, 197001 (2015).

18. D. F. Agterberg, D. S. Melchert, M. K. Kashyap, Emergent loop current order from pair density wave superconductivity. *Phys. Rev. B* **91**, 054502 (2015).

19. M. Zelli, C. Kallin, A. J. Berlinsky, Mixed state of a π-striped superconductor. *Phys. Rev. B* **84**, 174525 (2011).

20. M. Zelli, C. Kallin, A. J. Berlinsky, Quantum oscillations in a π-striped superconductor. *Physical Review B* **86**, 104507 (2012).

21. M. R. Norman, J. C. S. Davis, Quantum oscillations in a biaxial pair density wave state. *Proceedings of the National Academy of Sciences* **115**, 5389–5391 (2018).

22. Z. Dai, Y.-H. Zhang, T. Senthil, P. A. Lee, Pair-density waves, charge-density waves, and vortices in high-T_c cuprates. *Phys. Rev. B* **97**, 174511 (2018).

23. F. Yu, M. Hirschberger, T. Loew, G. Li, B. J. Lawson, T. Asaba, J. B. Kemper, T. Liang, J. Porras, G. S. Boebinger, J. Singleton, B. Keimer, L. Li, N. P. Ong, Magnetic phase diagram of underdoped YBa2Cu3Oy inferred from torque magnetization and thermal conductivity. *Proceedings of the National Academy of Sciences* **113**, 12667–12672 (2016).

24. M. H. Hamidian, S. D. Edkins, S. H. Joo, A. Kostin, H. Eisaki, S. Uchida, M. J. Lawler, E.-A. Kim, A. P. Mackenzie, K. Fujita, J. Lee, J. C. S. Davis, Detection of a Cooper-pair density wave in $Bi_2Sr_2CaCu_2O_{8+x}$. *Nature* **532**, 343–347 (2016).

25. T. Wu, H. Mayaffre, S. Kr¨amer, M. Horvati´c, C. Berthier, W. N. Hardy, R. Liang, D. a. Bonn, M.-H. Julien, Magnetic-field-induced charge-stripe order in the high-temperature superconductor $YBa_2Cu_3O_y$. *Nature* **477**, 191–194 (2011).

26. J. Chang, E. Blackburn, A. T. Holmes, N. B. Christensen, J. Larsen, J. Mesot, R. Liang, D. A. Bonn, W. N. Hardy, A. Watenphul, M. Zimmermann, E. M. Forgan, S. M. Hayden, Direct

observation of competition between superconductivity and charge density wave order in Y $YBa_2Cu_3O_y$. *Nature Physics* **8**, 871–876 (2012).

27. D. LeBoeuf, S. Krämer, W. N. Hardy, R. Liang, D. a. Bonn, C. Proust, Thermodynamic phase diagram of static charge order in underdoped $YBa_2Cu_3O_y$. *Nature Physics* **9**, 79–83 (2012).

28. S. Blanco-Canosa, A. Frano, T. Loew, Y. Lu, J. Porras, G. Ghiringhelli, M. Minola, C. Mazzoli, L. Braicovich, E. Schierle, E. Weschke, M. Le Tacon, B. Keimer, Momentum-dependent charge correlations in $YBa_2Cu_3O_{6+\delta}$ superconductors probed by resonant x-ray scattering: Evidence for three competing phases. *Physical Review Letters* **110**, 187001 (2013).

29. T. Wu, H. Mayaffre, S. Kr¨amer, M. Horvati´c, C. Berthier, W. Hardy, R. Liang, D. Bonn, M.-H. Julien, Incipient charge order observed by NMR in the normal state of $YBa_2Cu_3O_y$. *Nature Communications* **6**, 6438 (2015).

30. S. Gerber, H. Jang, H. Nojiri, S. Matsuzawa, H. Yasumura, D. A. Bonn, R. Liang, W. N. Hardy, Z. Islam, A. Mehta, S. Song, M. Sikorski, D. Stefanescu, Y. Feng, S. A. Kivelson, T. P. Devereaux, Z.-X. Shen, C.-C. Kao, W.-S. Lee, D. Zhu, J.-S. Lee, Three-dimensional charge density wave order in $YBa_2Cu_3O_{6.67}$ at high magnetic fields. *Science* **350**, 949–952 (2015).

31. J. Chang, E. Blackburn, O. Ivashko, a. T. Holmes, N. B. Christensen, M. H¨ucker, R. Liang, D. a. Bonn, W. N. Hardy, U. R¨utt, M. V. Zimmermann, E. M. Forgan, S. M. Hayden, Magnetic field controlled charge density wave coupling in underdoped $YBa_2Cu_3O_{6+x}$. *Nature Communications* **7**, 11494 (2016).

32. H. Jang, W.-S. Lee, H. Nojiri, S. Matsuzawa, H. Yasumura, L. Nie, A. V. Maharaj, S. Gerber, Y.-J. Liu, A. Mehta, D. A. Bonn, R. Liang, W. N. Hardy, C. A. Burns, Z. Islam, S. Song, J. Hastings, T. P. Devereaux, Z.-X. Shen, S. A. Kivelson, C.-C. Kao, D. Zhu, J.-S. Lee, Ideal charge-density-wave order in the high-field state of superconducting YBCO. *Proceedings of the National Academy of Sciences* **113**, 14645–14650 (2016).

33. B. Vignolle, D. Vignolles, M.-H. Julien, C. Proust, From quantum oscillations to charge order in highcopper oxides in high magnetic fields. *Comptes Rendus Physique* **14**, 39–52 (2013).

34. S. E. Sebastian, C. Proust, Quantum oscillations in hole-doped cuprates. *Annual Review of Condensed Matter Physics* **6**, 411–430 (2015).

35. J. E. Hoffman, E. W. Hudson, K. M. Lang, V. Madhavan, H. Eisaki, S. Uchida, J. C. Davis, A four unit cell periodic pattern of quasi-particle states surrounding vortex cores in $Bi_2Sr_2CaCu_2O_{8+\delta}$. *Science* **295**, 466–469 (2002).

36. K. Matsuba, S. Yoshizawa, Y. Mochizuki, T. Mochiku, K. Hirata, N. Nishida, Anti-phase Modulation of Electron- and Hole-like States in Vortex Core of $Bi_2Sr_2CaCu_2O_x$ Probed by

Scanning Tunneling Spectroscopy. *Journal of the Physical Society of Japan* **76**, 063704 (2007).

37. S. Yoshizawa, T. Koseki, K. Matsuba, T. Mochiku, K. Hirata, N. Nishida, High-Resolution Scanning Tunneling Spectroscopy of Vortex Cores in Inhomogeneous Electronic States of $Bi_2Sr_2CaCu_2O_x$. *Journal of the Physical Society of Japan* **82**, 083706 (2013).

38. T. Machida, Y. Kohsaka, K. Matsuoka, K. Iwaya, T. Hanaguri, T. Tamegai, Bipartite electronic superstructures in the vortex core of $Bi_2Sr_2CaCu_2O_{8+\delta}$. *Nature Communications* **7**, 11747 (2016).

39. S. A. Kivelson, D.-h. Lee, E. Fradkin, V. Oganesyan, Competing order in the mixed state of hightemperature superconductors. *Physical Review B* **66**, 144516 (2002).

40. D. F. Agterberg, H. Tsunetsugu, Dislocations and vortices in pair density wave superconductors. *Nature Physics* **4**, 639–642 (2009).

41. J. D. Sau, S. Sachdev, Mean-field theory of competing orders in metals with antiferromagnetic exchange interactions. *Phys. Rev. B* **89**, 075129 (2014).

42. M. Einenkel, H. Meier, C. P´epin, K. B. Efetov, Vortices and charge order in high-Tc superconductors. *Phys. Rev. B* **90**, 054511 (2014).

43. Y. Wang, S. D. Edkins, M. H. Hamidian, J. C. S. Davis, E. Fradkin, S. A. Kivelson, Pair density waves in superconducting vortex halos. *Phys. Rev. B* **97**, 174510 (2018).

44. Materials and methods are available as supplementary materials.

45. M. H. Hamidian, S. D. Edkins, C. K. Kim, J. C. Davis, A. P. Mackenzie, H. Eisaki, S. Uchida, M. J. Lawler, E. A. Kim, S. Sachdev, K. Fujita, Atomic-scale electronic structure of the cuprate d-symmetry form factor density wave state. *Nature Physics* **12**, 150–156 (2016).

46. M. J. Lawler, K. Fujita, J. Lee, a. R. Schmidt, Y. Kohsaka, C. K. Kim, H. Eisaki, S. Uchida, J. C. Davis, J. P. Sethna, E.-A. Kim, Intra-unit-cell electronic nematicity of the high-Tc copper-oxide pseudogap states. *Nature* **466**, 347–351 (2010).

47. N. Schopohl, K. Maki, Quasiparticle spectrum around a vortex line in a d-wave superconductor. *Phys. Rev. B* **52**, 490–493 (1995).

48. M. Ichioka, N. Hayashi, N. Enomoto, K. Machida, Vortex structure in d-wave superconductors. *Phys. Rev. B* **53**, 15316–15326 (1996).

49. M. Franz, C. Kallin, P. I. Soininen, A. J. Berlinsky, A. L. Fetter, Vortex state in a d-wave superconductor. *Phys. Rev. B* **53**, 5795–5814 (1996).

50. Y. Morita, M. Kohmoto, K. Maki, Quasiparticle Spectra around a Single Vortex in a d-Wave Superconductor. *Phys. Rev. Lett*. **78**, 4841–4844 (1997).

51. M. Franz, Z. Tešanović, Self-consistent electronic structure of a $d_{x^2-y^2}$ and a $d_{x^2-y^2} + id_{xy}$ vortex*. Phys. Rev. Lett*. **80**, 4763–4766 (1998).

52. H. Nishimori, K. Uchiyama, S.-i. Kaneko, A. Tokura, H. Takeya, K. Hirata, N. Nishida, First Observation of the fourfold-symmetric and quantum regime vortex core in YNi_2B_2C by scanning tunneling microscopy and spectroscopy. *Journal of the Physics Society Japan* **73**, 3247–3250 (2004).

53. H. Sakata, M. Oosawa, K. Matsuba, N. Nishida, H. Takeya, K. Hirata, Imaging of a Vortex Lattice Transition in YNi_2B_2C by Scanning Tunneling Spectroscopy. *Physical Review Letters* **84**, 1583–1586 (2000).

54. T. Klein, I. Joumard, S. Blanchard, J. Marcus, R. Cubitt, T. Giamarchi, P. Le Doussal, A Bragg glass phase in the vortex lattice of a type II superconductor. *Nature* **413**, 404–406 (2001).

55. A. J. Macdonald, Y. S. Tremblay-Johnston, S. Grothe, S. Chi, P. Dosanjh, S. Johnston, S. A. Burke, Dispersing artifacts in FT-STS: A comparison of set point effects across acquisition modes. *Nanotechnology* **27**, 414004 (2016).

56. J. Robertson, S. Kivelson, E. Fradkin, A. Fang, A. Kapitulnik, Distinguishing patterns of charge order: Stripes or checkerboards. *Physical Review B* **74**, 134507 (2006).

Acknowledgements:

We acknowledge and thank D. Agterberg, P. Choubey, A. Chubukov, E. Fradkin, P.J. Hirschfeld, P.D. Johnson, D.H. Lee, P.A. Lee, C. Pepin, S. Sebastian, S. Todadri, J. Tranquada and Yuxuan Wang, for helpful discussions, advice and communications. We are grateful to S. A. Kivelson for crucial proposals on the complete set of PDW phenomena to search for within the vortex halo.

Funding: S.U. and H.E. acknowledge support from a Grant-in-Aid for Scientific Research from the Ministry of Science and Education (Japan); A.K., and K.F. acknowledge salary support from the U.S. Department of Energy, Office of Basic Energy Sciences, under contract number DEAC02-98CH10886. E-AK acknowledges support from the U.S. Department of Energy, Office of Basic Energy Sciences under award ID**:** DE-SC0018946. SS acknowledges support under National Science Foundation under Grant No. DMR- 1664842. J.C.S.D., S.D.E. and M.H.H. acknowledge support from the Moore Foundation's EPiQS Initiative through Grant GBMF4544.

Author Contributions: S.D.E., A.K. and M.H.H. carried out the experiments; K.F., H.E. and S.U. synthesized and characterized the samples; M.H.H., S.D.E. and K.F. developed and carried out analysis; S.S., M.L. and E.-A.K. provided theoretical guidance; A.P.M. and J.C.D. supervised the project and wrote the paper with key contributions from S.D.E., K.F and M.H.H. The manuscript reflects the contributions and ideas of all authors.

Competing interests: The authors declare no competing financial interests.

Data and materials availability:
The data files for the results presented here and the codes used in their analysis are available at:
https://dataverse.harvard.edu/dataset.xhtml?persistentId=doi:10.7910/DVN/JDSN1W

Supplementary Materials:
Materials and Methods
Supplementary Text
Figs. S1 to S8
References *(46-56)*

FIGURE CAPTIONS

Figure 1 Schematic of Field-induced Unidirectional $8a_0$ Pair Density Wave

A. Diagram of the halo region (grey) surrounding the vortex core (black) of a cuprate superconductor (SC). The CuO_2 plane orientation and Cu-Cu periodicity are indicating by using a dot for each Cu site. Within the halo, a unidirectional PDW modulation along the x-axis with periodicity $8a_0$, characterized by an order parameter $\Delta_P^Q(r)$ shown as red curve in the upper graph, is indicated schematically by red shading.

B. Solid curve: Envelope containing non-zero amplitude $\Delta_P^Q\Delta_{SC}^*$ of the $N(\boldsymbol{r})$ modulations caused by the interaction between the SC and PDW order parameters, plotted along the fine horizontal line in (A) through the vortex core. Dashed curve: The envelope containing non-zero amplitude $\Delta_P^{-Q}\Delta_P^{Q\,*}$ of the $N(\boldsymbol{r})$ modulations caused by PDW itself, plotted along the same fine line. For clarity, we ignore the small region (less than 1nm) at the core where $\Delta_P^Q\Delta_{SC}^*$ must rise from zero as Δ_{SC} does.

C. Within a G-L model, if the field-induced PDW has a pure d-symmetry form factor, $F_P = F_d$, then two sets of $N(\boldsymbol{r})$ modulations should appear together. The first is $N(\boldsymbol{r}) \propto cos(\boldsymbol{Q_P}.\boldsymbol{r})$ caused by $\Delta_P^Q\Delta_S^*$ and indicated in $\widetilde{N}(\boldsymbol{q})$ (the Fourier transform of $N(\boldsymbol{r})$) by a solid red curve. The second $N(\boldsymbol{r}) \propto cos(2\boldsymbol{Q_P}.\boldsymbol{r})$ caused by $\Delta_P^{-Q}\Delta_P^{Q\,*}$ is indicated in $\widetilde{N}(\boldsymbol{q})$ by a dashed red curve. The decay length for the $\boldsymbol{2Q_P}$ modulation should be half that of the $\boldsymbol{Q_P}$ modulation, meaning that the linewidth $\delta 2Q_P$ of the $\boldsymbol{2Q_P}$ modulation (dashed red) should be twice that of the $\boldsymbol{Q_P}$ modulation, δQ_P (solid red). If the PDW has a pure s-symmetry form factor, $F_P = F_s$, then a different pair of $N(\boldsymbol{r})$ modulations should appear together. First is $N(\boldsymbol{r}) \propto cos((\boldsymbol{Q_B} - \boldsymbol{Q_P}) \cdot \boldsymbol{r})$ caused by $\Delta_P^{-Q}\Delta_S^*$ (solid blue line) and second $N(\boldsymbol{r}) \propto cos(2\boldsymbol{Q_P}) \cdot \boldsymbol{r})$ caused by $\Delta_P^{-Q}\Delta_P^{Q\,*}$ (dashed blue line). Here $\boldsymbol{Q_B}$ is the Bragg wavevector of the CuO_2 unit cell.

Figure 2 Four-unit-cell Quasiparticle Modulations at Vortex Halos in $Bi_2Sr_2CaCu_2O_8$

A. Topographic image $T(\boldsymbol{r})$ of BiO termination layer of our $Bi_2Sr_2CaCu_2O_8$ sample. The displacement of every specific atomic site in this field of view between zero field and B=8.25 Tesla was constrained by post processing of all low/high field data sets to be less than 10 pm (Section 3, Ref. 45).

B. Measured differential tunnel conductance spectrum $g(\boldsymbol{r}, E = eV) \equiv dI/dV(\boldsymbol{r}, V)$ showing how to identify the symmetry point of a vortex core (dashed line). The full line shows measured $g(\boldsymbol{r}, E = eV)$ at the identical location in zero field. Yellow shaded region indicates low energy Bogoliubov quasiparticle states generated by the vortex.

C. Measured $\delta g(\boldsymbol{r}, 12meV) = g(\boldsymbol{r}, 12meV, B = 8.25T) - g(\boldsymbol{r}, 12meV, B = 0)$ showing typical examples of the low-energy Bogoliubov quasiparticle modulations (Refs 35-38) within halo regions surrounding four vortex cores in $Bi_2Sr_2CaCu_2O_8$.

Figure 3 Field-induced s-symmetry Form Factor Modulations within Vortex Halos

(A) Measured field-induced modulations $\delta g(\boldsymbol{r}, 30meV) = g(\boldsymbol{r}, 30meV, B = 8.25T) - g(\boldsymbol{r}, 30meV, B = 0)$ in a 58nm X 58nm FOV. The simultaneously measured topographs $T(\boldsymbol{r})$ at B=8.25T and 0T are shown in Section 3 , Fig. S2, Ref. **Error! Bookmark not defined.**, and demonstrate by the absence of local maxima at $\boldsymbol{q} \approx [(\pm 1/8, 0); (0, \pm 1/8)]2\pi/a_0$ in their Fourier transforms that the setup effect is not influencing observations of $\delta g(\boldsymbol{r}, E)$ modulations at these wavevectors (Section 5 Ref. **Error! Bookmark not defined.**).

(B) Amplitude Fourier transform $|\widetilde{\delta g}(\boldsymbol{q}, 30meV)|$ (square root of power spectral density) of $\delta g(\boldsymbol{r}, 30meV)$ data in A. The $\boldsymbol{q} = (\pm 1/4, 0); (0, \pm 1/4)2\pi/a_0$ points are indicated by black crosses. Four sharp maxima, indicated by $\boldsymbol{Q_P}$, occur at $\boldsymbol{q} \approx [(\pm 1/8, 0); (0, \pm 1/8)]2\pi/a_0$ whereas four broader maxima, indicated by $\boldsymbol{2Q_P}$, occur at $\boldsymbol{q} \approx [(\pm 1/4, 0); (0, \pm 1/4)]2\pi/a_0$.

(C) Measured amplitude envelope of the modulations in $\delta g(\boldsymbol{r}, 30meV)$ at $\boldsymbol{Q_P}$ showing that they only occur within the vortex halo regions.

(D) Measured amplitude envelope of the modulations in $\delta g(\boldsymbol{r}, 30meV)$ at $\boldsymbol{2Q_P}$ showing that they also only occur within the vortex halo regions.

(E) Measured $|\widetilde{\delta g}(\boldsymbol{q}, 30meV)|$ along (0,0)-(1/2,0) (dashed line in B) showing the two maxima in the field induced $N(\boldsymbol{r})$modulations, occurring at by $\boldsymbol{Q_P} = 0.117 \pm 0.01$ and $\boldsymbol{2Q_P} = 0.231 \pm 0.01$ (see Fig. 4A-D)

(F) Amplitude Fourier transform of the d-symmetry form factor modulations in $N(\boldsymbol{r})$ $|\widetilde{D}^{\delta g}(\boldsymbol{q}, 30meV)|$ derived from measured $\delta g(\boldsymbol{r}, 30meV)$ data in 3A. Again, $\boldsymbol{q} = (\pm 1/4, 0); (0, \pm 1/4)2\pi/a_0$ points are indicated by black crosses. Two maxima, labeled as $\boldsymbol{Q_P}$, occur at $\boldsymbol{q} \approx [(\pm 1/8, 0); (0, \pm 1/8)]2\pi/a_0$ whereas two broader maxima, indicated by $\boldsymbol{2Q_P}$, occur at $\boldsymbol{q} \approx [(\pm 1/4, 0); (0, \pm 1/4)]2\pi/a_0$, both sets oriented along the y-axis.

(G) Measured $|\widetilde{D}^{\delta g}(\boldsymbol{q}, 30meV)|$ along (0,0)-(1/2,0) (dashed line in 3F) showing the maxima in the field induced $N(\boldsymbol{r})$ modulations occurring at $\boldsymbol{Q_P}$ and $\boldsymbol{2Q_P}$. A unidirectional d-symmetry form factor change density modulation, as observed extensively in zero field (*46*), would have such characteristics, as would contributions from an s-symmetry form factor PDW. These modulations did not appear in Fig. 3 because, in that unprocessed $\delta g(\boldsymbol{r}, E)$ data, they occur at $\boldsymbol{Q} \approx (0, \pm 7/8)2\pi/a_0$ and $\boldsymbol{Q} \approx (0, \pm 3/4)2\pi/a_0$ owing to their d-symmetry form factor (see Figs 4A-D).

Figure 4 Field-induced $N(\boldsymbol{r})$ Modulations indicative of a PDW state in the Vortex Halo

(A, B) Amplitude Fourier transform $|\widetilde{\delta g}(\boldsymbol{q}, 30meV)|$ derived from $\delta g(\boldsymbol{r}, 30meV)$ data is plotted along two orthogonal axes from (0,0)-(0,1) and (00)-(1,0), to reach both Bragg points. All four local maxima, at $\boldsymbol{Q_P}$ and $\boldsymbol{2Q_P}$ from the *s*-symmetry field-induced $N(\boldsymbol{r})$ modulations, plus at $\boldsymbol{1-Q_P}$ and $\boldsymbol{1-2Q_P}$ from the *d*-symmetry field-induced $N(\boldsymbol{r})$ modulations, may be seen. Measurement from these fits of the q-magnitude and width δq of the *s*-symmetry peaks at $\boldsymbol{Q_P}$ and $\boldsymbol{2Q_P}$ yields: $Q_P^x = 0.117, Q_P^y = 0.129$; $2Q_P^x = 0.231, 2Q_P^y = 0.237$; $\delta Q_P^x = 0.020$, $\delta Q_P^y = 0.020$; $\delta 2Q_P^x = 0.034$, $\delta 2Q_P^y = 0.035$. Inset shows $|\widetilde{\delta g}(\boldsymbol{q}, 30meV)|$.

(C, D) As in (A, B) but at E=-30 meV. Measurement yield : $Q_P^x = 0.115, Q_P^y = 0.128$; $2Q_P^x = 0.239, 2Q_P^y = 0.235$; $\delta Q_P^x = 0.020$, $\delta Q_P^y = 0.020$; $\delta 2Q_P^x = 0.039$, $\delta 2Q_P^y = 0.045$. Inset shows $|\widetilde{\delta g}(\boldsymbol{q}, -30meV)|$. The *s*-symmetry field-induced $N(\boldsymbol{r})$ modulations at $\boldsymbol{Q_P}$ and $\boldsymbol{2Q_P}$ are almost perfectly particle-hole symmetric (insets B,D) in the sense that $N(\boldsymbol{r}, E > 25meV) = N(\boldsymbol{r}, E < -25meV)$ for these two wavevectors.

(E) Fourier transform $\widetilde{\delta\Delta}(\boldsymbol{q})$ of measured $\delta\Delta(\boldsymbol{r}) = \Delta(\boldsymbol{r}, 8.25\mathrm{T}) - \Delta(\boldsymbol{r}, 0)$) (Section 7 of Ref. 45). The observed peaks revealing field-induced gap modulation occur at points indistinguishable from $\boldsymbol{Q_P}$**.** The peak along the (1,1) direction occurs at the wavevector of the crystal supermodulation, where a modulation induced PDW has long been identified.

(F) Schematic representation of a bi-directional PDW with a *d*-symmetry form factor induced within a vortex halo that is consonant with the data in this paper when considered in the context of vortex halo theory (*5,43,44*).

FIG 1

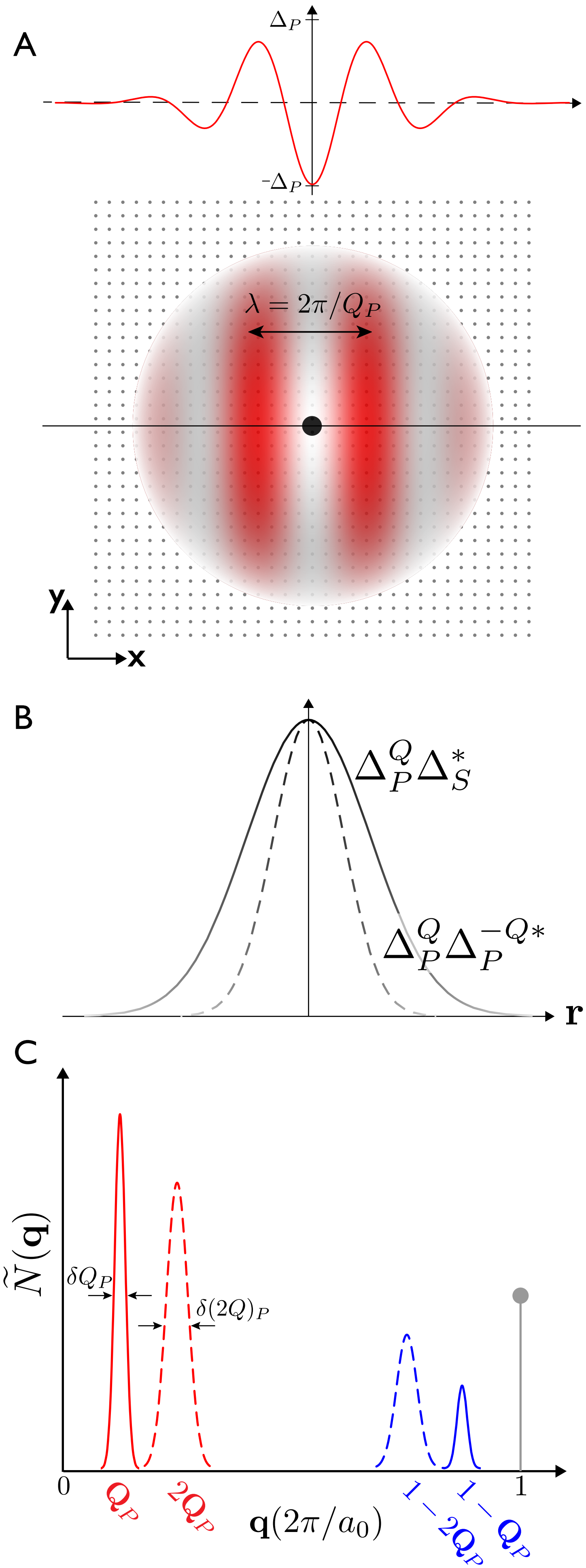

A
Δ_P
-Δ_P
$\lambda = 2\pi/Q_P$
y
x
B
$\Delta_P^Q \Delta_S^*$
$\Delta_P^Q \Delta_P^{-Q*}$
r
C
$\widetilde{N}(\mathbf{q})$
δQ_P
$\delta(2Q)_P$
0
$\mathbf{Q}_P$
$2\mathbf{Q}_P$
$\mathbf{q}(2\pi/a_0)$
$1-2\mathbf{Q}_P$
$1-\mathbf{Q}_P$
1

FIG 2

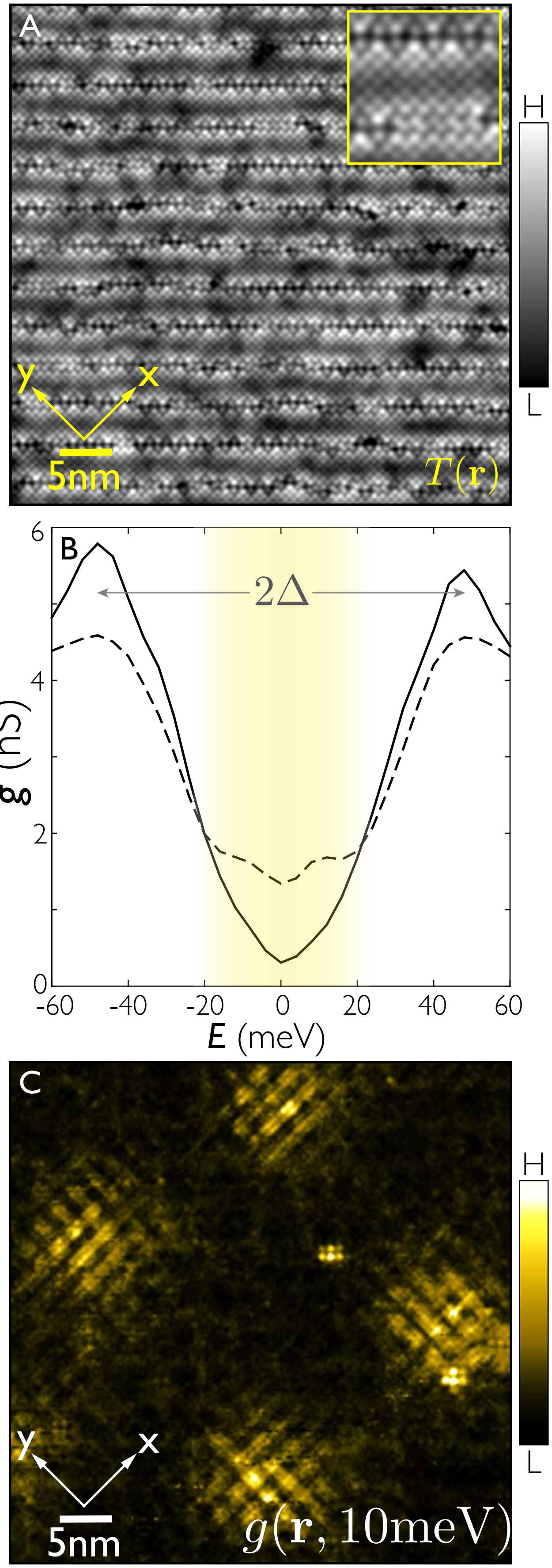

A
H
L
y
x
5nm
$T(\mathbf{r})$
B
2Δ
g (nS)
6
4
2
0
-60
-40
-20
0
20
40
60
E (meV)
C
H
L
y
x
5nm
$g(\mathbf{r}, 10\text{meV})$

FIG 3

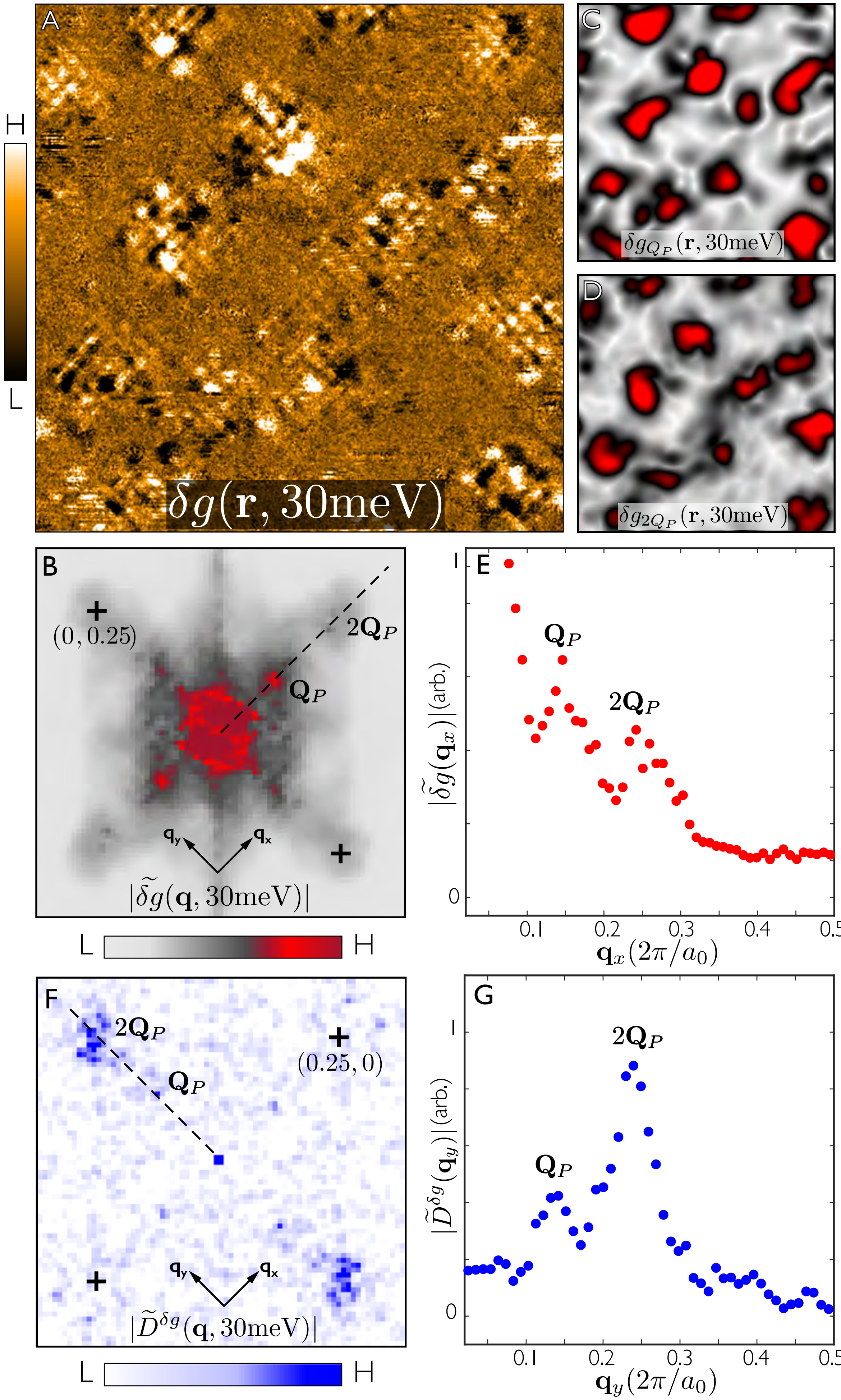

A
H
L
$\delta g(\mathbf{r}, 30\text{meV})$
C
$\delta g_{Q_P}(\mathbf{r}, 30\text{meV})$
D
$\delta g_{2Q_P}(\mathbf{r}, 30\text{meV})$
H
L
B
$(0, 0.25)$
$2\mathbf{Q}_P$
$\mathbf{Q}_P$
$\mathbf{q}_y$
$\mathbf{q}_x$
$|\widetilde{\delta g}(\mathbf{q}, 30\text{meV})|$
L
H
E
$\mathbf{Q}_P$
$2\mathbf{Q}_P$
$|\widetilde{\delta g}(\mathbf{q}_x)|$ (arb.)
1
0
0.1
0.2
0.3
0.4
0.5
$\mathbf{q}_x(2\pi/a_0)$
F
$2\mathbf{Q}_P$
$\mathbf{Q}_P$
$(0.25, 0)$
$\mathbf{q}_y$
$\mathbf{q}_x$
$|\widetilde{D}^{\delta g}(\mathbf{q}, 30\text{meV})|$
L
H
G
$2\mathbf{Q}_P$
$\mathbf{Q}_P$
$|\widetilde{D}^{\delta g}(\mathbf{q}_y)|$ (arb.)
1
0
0.1
0.2
0.3
0.4
0.5
$\mathbf{q}_y(2\pi/a_0)$

FIG 4

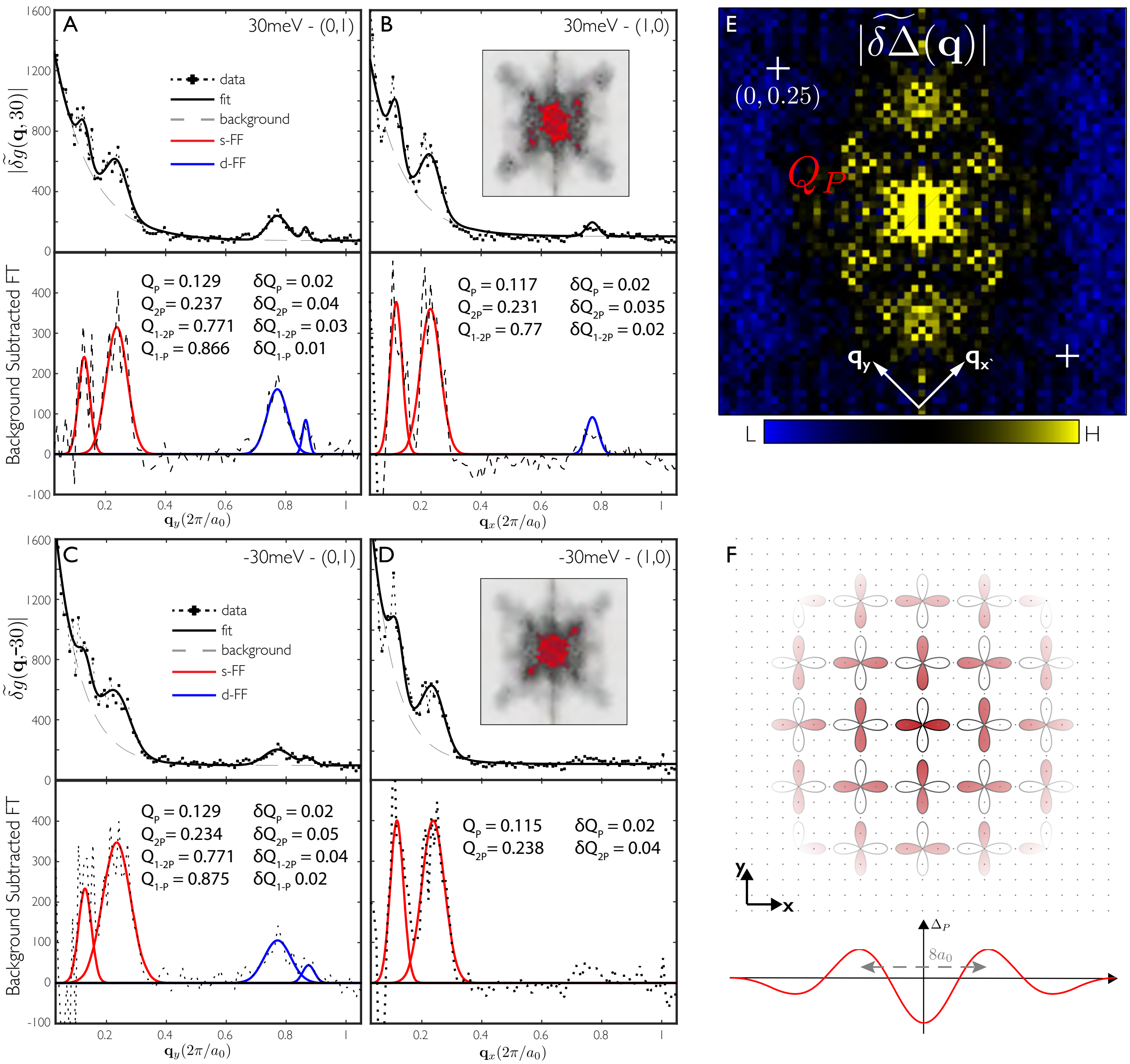

A
30meV - (0,1)
data
fit
background
s-FF
d-FF
$|\tilde{\delta g}(\mathbf{q}, 30)|$
Background Subtracted FT
$Q_P = 0.129$ $\delta Q_P = 0.02$
$Q_{2P} = 0.237$ $\delta Q_{2P} = 0.04$
$Q_{1\text{-}2P} = 0.771$ $\delta Q_{1\text{-}2P} = 0.03$
$Q_{1\text{-}P} = 0.866$ $\delta Q_{1\text{-}P}$ 0.01
$\mathbf{q}_y(2\pi/a_0)$
B
30meV - (1,0)
$Q_P = 0.117$ $\delta Q_P = 0.02$
$Q_{2P} = 0.231$ $\delta Q_{2P} = 0.035$
$Q_{1\text{-}2P} = 0.77$ $\delta Q_{1\text{-}2P} = 0.02$
$\mathbf{q}_x(2\pi/a_0)$
E
$|\widetilde{\delta\Delta}(\mathbf{q})|$
(0, 0.25)
Q_P
$\mathbf{q_y}$
$\mathbf{q_x}$
L
H
C
-30meV - (0,1)
data
fit
background
s-FF
d-FF
$\tilde{\delta g}(\mathbf{q}, \text{-}30)|$
Background Subtracted FT
$Q_P = 0.129$ $\delta Q_P = 0.02$
$Q_{2P} = 0.234$ $\delta Q_{2P} = 0.05$
$Q_{1\text{-}2P} = 0.771$ $\delta Q_{1\text{-}2P} = 0.04$
$Q_{1\text{-}P} = 0.875$ $\delta Q_{1\text{-}P}$ 0.02
$\mathbf{q}_y(2\pi/a_0)$
D
-30meV - (1,0)
$Q_P = 0.115$ $\delta Q_P = 0.02$
$Q_{2P} = 0.238$ $\delta Q_{2P} = 0.04$
$\mathbf{q}_x(2\pi/a_0)$
F
y
x
Δ_P
$8a_0$

Science
AAAS

Supplementary Materials for

Magnetic-field Induced Pair Density Wave State in the Cuprate Vortex Halo

S.D. Edkins, A. Kostin, K. Fujita, A. P. Mackenzie, H. Eisaki, S. Uchida, Subir Sachdev, M.J. Lawler, E-A. Kim, J.C. Séamus Davis, and M. H. Hamidian

Correspondence to: jcseamusdavis@gmail.com and m.hamidian@gmail.com

This PDF file includes:

Materials and Methods

For our studies, high-quality $Bi_2SrCaCu_2O_{8+\delta}$ single crystals were grown using the travelling-solvent-floating zone (TSFZ) method. The samples are of $Bi_{2.1}Sr_{1.9}CaCu_2O_{8+\delta}$ and were synthesized from dried powders of Bi_2O_3, $SrCO_3$, $CaCO_3$ and CuO. The crystal growth was carried out in air and at growth speeds of 0.15-0.2 mm/h for all samples. Inductively coupled plasma (ICP) spectroscopy was used for the composition analysis and a vibrating sample magnetometer (VSM) was used for measurement of T_c. Here we studied samples of $Bi_2SrCaCu_2O_{8+\delta}$ with hole doping p $\approx$ 0.17. Each sample was inserted into the cryogenic ultra high vacuum of the SI-STM system and cleaved to reveal an atomically flat BiO surface. All measurements were performed at a temperature of 2K. The basic spectroscopic imaging STM consists of lock-in amplifier measurements of the differential tunneling conductance with sub-unit-cell resolution and register, as a function of both location $\mathbf{r}$ and electron energy E. We vary the applied magnetic field perpendicular to the CuO_2 planes of the samples using a superconducting solenoid with a highly stable persistent current/field.

Supplementary Text

1. Order Parameter Description of Pair Density Waves

Phenomenologically one can describe pair density wave (PDW) states by expanding the pairing amplitude in order parameters,

$$\Delta_{PD}(\mathbf{r}_1,\mathbf{r}_2) = \langle \hat{\psi}^\dagger_\sigma(\mathbf{r}_1)\hat{\psi}^\dagger_{-\sigma}(\mathbf{r}_2)\rangle = F(\mathbf{r}_1-\mathbf{r}_2)\left[\Delta_P^{\mathbf{Q_x}}(\mathbf{r})e^{i\mathbf{Q_x}\cdot\mathbf{r}} + \Delta_P^{-\mathbf{Q_x}}(\mathbf{r})e^{-i\mathbf{Q_x}\cdot\mathbf{r}} + \Delta_P^{\mathbf{Q_y}}(\mathbf{r})e^{i\mathbf{Q_y}\cdot\mathbf{r}} + \Delta_P^{-\mathbf{Q_y}}(\mathbf{r})e^{-i\mathbf{Q_y}\cdot\mathbf{r}}\right] , \tag{S1}$$

where $\hat{\psi}^\dagger_\sigma(\mathbf{r}_1)$ creates a quasi-particle of spin σ at location $\mathbf{r}_1$ and $\mathbf{r} = (\mathbf{r}_1+\mathbf{r}_2)/2$. $\Delta_P^{\mathbf{Q_x}}$ and $\Delta_P^{\mathbf{Q_y}}$ are PDW order parameters. They are complex scalar fields which carry momenta $\mathbf{Q_x}$ and $\mathbf{Q_y}$ running along orthogonal directions $\mathbf{x}$ and $\mathbf{y}$.

Here we have chosen to consider a tetragonal system with quasi two-dimensional order so that the PDW wave-vectors lie in the square planes of the tetragonal lattice. We will first consider PDW with axial wave-vectors $\mathbf{Q}_{\pm\mathbf{x}}$ and $\mathbf{Q}_{\pm\mathbf{y}}$ that run along the two symmetry equivalent Cu-O directions in the CuO_2 planes.

The function $F(\mathbf{r}_1-\mathbf{r}_2)$ is the form factor of the PDW. Because the axial wave-vectors break rotational symmetry means the form factors are not themselves sufficient to determine which irreducible representation of the point group the PDW transforms as. However, if $F(\mathbf{r}_1-\mathbf{r}_2)$ is even under 90° rotation then the PDW can be termed to have an s-wave form factor whereas if it is odd it has a d-wave form factor.

2. Induced Orders at Superconducting Vortex

In this section we describe how an order parameter that competes with superconductivity can be induced at superconducting vortices. Following reference (*39*), the Ginzburg-Landau free energy functional describing the competition between uniform superconductivity and another order parameter is given by

$$\mathcal{F}[\Delta_{SC},\Delta_A] = \mathcal{F}_{\Delta_{SC}}[\Delta_{SC}] + \mathcal{F}_{\Delta_A}[\Delta_A] + u_1|\Delta_{SC}|^2|\Delta_A|^2 + ..., \tag{S2}$$

where Δ_{SC} is a complex scalar field representing the uniform superconducting order parameter and and Δ_A is a field representing a competing order such as PDW or CDW. For the case of competing order we focus on here $u_1 > 0$.

The superconducting contribution to the free energy is given by its usual form

$$\mathcal{F}[\Delta_{SC}] = \frac{\kappa_0}{2}\left|\left(\frac{\nabla}{i} - \frac{2e}{c}\mathbf{A}\right)\Delta_{SC}\right|^2 - \frac{\kappa_0}{4\xi^2}|\Delta_{SC}|^2 + \frac{1}{4}|\Delta_{SC}|^4 + ... \tag{S3}$$

where $\mathbf{A}$ is the magnetic vector potential and ξ is the superconducting coherence length. The contribution from the competing order is given by

$$\mathcal{F}_{\Delta_A}[\phi] = \frac{\kappa_{\Delta_A}}{2}|\nabla\Delta_A|^2 + \frac{\alpha}{2}|\Delta_A|^2 + \frac{1}{4}|\Delta_A|^4 + ... \; . \tag{S4}$$

It is shown in reference (*39*) that if and only if the subdominant competing order is sufficiently close in free energy density to the uniform superconducting phase is there a halo around superconducting vortices where the two orders coexist. Such a near degeneracy between uniform superconductivity and 8a0 PDW (and lack thereof with 8a0 CDW) has been demonstrated in numerical studies of the t-J model (*10*). Moreover, the other alternative that a $8a_0$ SDW order is induced is ruled out by lack of such signatures in field-dependent neutron scattering.

3. Enhanced Measurement and Analysis Techniques

Our experiments follow, at an essential level, the same procedure as employed in the classic "Hoffman" experiments in which $g(\mathbf{r}, E)$ is measured at zero field and then at high magnetic field B in the identical FOV using an identical STM tip. The former is subtracted from the latter to yield the field-induced changes $\delta g(r, E, B)$.

In order to detect the field induced PDW described in the main text, it was necessary to go substantially beyond these initial experiments in the complexity of both experimental data acquisition and analysis. Specifically, we enhance both the r-space resolution using smaller pixels and the q-space resolution by using a larger FOV, increase the number of vortices per image, use distortion-corrected sublattice-phase-resolved imaging, and measure in a far wider energy range.

Figure S1 summarizes the new combination of capabilities employed: the field induced perturbation to the electronic density of states study $\delta g(\mathbf{r}, E, B)$ is measured in a large FOV with sub-unit-cell resolution. All data are processed using the Lawler-Fujita algorithm (*46*) to render all $T(\mathbf{r}, V)$ and all $g(\mathbf{r}, E, B)$ distortion free and identically periodic; this approach automatically generates sublattice-phase-resolved data sets g(r,E,B) so that the structure factor of all modulations becomes available (*45*). After these steps, the $\delta g(\mathbf{r}, E, B)$ field induced electronic structure changes are measured in a wide range of energies E, from the gap node to beyond the gap edge.

The field on/off subtraction that was key to our studies relies on spatial registration of the two data sets to be subtracted. To demonstrate the high precision of spatial registration between the data sets taken at $B = 0$T and $B = 8.25$T, we show in figure S2 the processed topographic images acquired simultaneously with the spectroscopic maps analyzed in the main text. These data sets were taken weeks apart in the same region of the sample. The raw data for all data sets were phase corrected using the Lawler-Fujita distortion-correction algorithm (*46*), mapping the data onto a perfectly periodic lattice free of lattice distortions due to systematic measurement effects. After this procedure the full-width at half-maximum of intensity at each Bragg point is $\delta_q \frac{2\pi}{a_0}$ where $\delta_q = 0.01$, as shown in figure 3. What this means is that, in a given $T(r, V)$ image, we can locate the center of each atom with precision of approximately $\delta_x \approx \delta_q a_0 = 0.01 \times 380\text{pm} = 3.8\text{pm}$.

A morphing scheme was then implemented to register all data sets in the same field of view (FOV) to one another. Given that the precision with which a give atom's center can be located in a single image is 3.8pm, the precision with which two atoms can be registered along a given axis is ≈ 8pm and $\sqrt{2} \times 8\text{pm} \approx 10$pm in a arbitrary direction. This method allows meaningful subtraction of high and low field data to detect magnetic field induced differences of the electronic structure at the sub-unit-cell scale.

4. Vortex Core and Halo

Early theories of high-T_c cuprate vortex structure predicted a peak in the density of states at the Fermi energy which, in real-space, is four-fold symmetric and decays algebraically along the directions the gap nodes(*47*–*51*). This structure arises in Bogoliubov de-Gennes theory of the d-wave vortex core because the line nodes preclude the formation of the Caroli de-Gennes Matricon bound states. While such four-fold symmetric zero-energy peaks are observed in highly anisotropic s-wave superconductors such as YNi_2B_2C (*52*, *53*), early STM studies of cuprate vortices did not reveal this phenomenology and instead observed periodic modulations of the density of states at energies in the range $E \sim 10$meV (*35*).

In keeping with previous vortex studies (*35*–*38*) we identify superconducting vortices in conductance images from 1) the suppression of coherence peaks and filling of the gap in the tunelling spectrum that occurs in a radius ~1nm around the center of the vortex and signifies its core (as shown in figure S4) 2) the periodic low energy quasi-particle modulations that identify the halo surrounding the core (as shown in figure S5). While these vortex signatures are visible without subtracting the $B = 0$T conductance from that at $B = 8.25$T, the $8a_0$ period spatial modulations at $|E| = 30$meV associated with the PDW are far smaller in magnitude and require the superior signal to noise ratio associated with the subtraction procedure to be detected.

In figure S6 we use yellow circles to identify vortex halos in the conductance images. The first thing to note is that, due to pinning disorder, there is no fully ordered vortex lattice. This vortex Bragg glass in $Bi_2Sr_2CaCu_2O_8$ is well known and in agreement with our own and others STM experiments (*35–38*, *54*). Secondly, we note that number of vortices in the field of view is, within statistical error, as expected. In a 58nm x 58nm FOV at B=8.25T we expect 14 vortices carrying a flux $\frac{h}{2e}$. As shown in figure S6 we observe 12 vortices clearly whose positions remains acceptably stable during the study period (yellow circles) . There are two regions that clearly contain the same compact field induced electronic structure modulations (red circles) but the position of these two vortex halos was not stable during the measurements. The horizontal streaking observed here (and in all other vortex halo studies) is an indication of changes of vortex position, and not of noise in measurement.

5. Absence of Influence from Setup Effect

All spectroscopic imaging STM experiments are affected by the so-called "setup effect". To understand this systematic effect and its consequences, consider the equation for the tip-sample tunneling current

$$I(\mathbf{r}, V) = \int_0^{eV} n(\mathbf{r}, E) n_t T(z, E) \mathrm{d}E \tag{S5}$$

where $n(\mathbf{r}, E)$ is the density-of-electronic-states at each location, $\mathbf{r}$, in the plane of the surface at energy E and n_t is the constant density-of-electronic-states in the tip. $T(z, V, E)$ is the coefficient controlling the magnitude of the tunneling current and depends on the tip-surface distance, z, and the bias voltage between tip and sample, V. To establish a certain "setup" tip-sample distance, z_s, the feedback loop is adjusted at the "setup voltage", V_s, until a pre-chosen but arbitary "setup current"

$$I_s(\mathbf{r}, V) = \int_0^{eV_s} n(\mathbf{r}, E) n_t T(z_s, E) \mathrm{d}E \tag{S6}$$

is achieved. The feedback is then disengaged and the tip-sample distance stabilized at z_s. Electron tunneling theory then predicts that in the limit where the work function $\phi \gg eV$

$$T(z_s, E) \propto e^{-\frac{-z}{z_0}}; z_0 \approx \hbar/2\sqrt{2m\phi} \tag{S7}$$

. In that case

$$I_s(\mathbf{r}, V) \approx Ce^{-\frac{-z}{z_0}} \int_0^{eV_s} n(\mathbf{r}, E) \mathrm{d}E \tag{S8}$$

where C is a constant. Therefore, the 2D function usually referred to as the constant-current topograph $z_s(\mathbf{r})$ is

$$\frac{z_s(\mathbf{r})}{z_0} = \log\left[\int_0^{eV_s} n(\mathbf{r}, E) \mathrm{d}E\right] + C' \tag{S9}$$

where C' is a constant. For this set of tip-surface distances, $z_s(\mathbf{r})$, Eqn. S5 then becomes $I(\mathbf{r}, V) \approx Ce^{-\frac{-z_s(\mathbf{r}}{z_0}} \int_0^{eV_s} n(\mathbf{r}, E) \mathrm{d}E$ so that the differential tunnelling conductance spectrum is given by

$$\left.\frac{dI}{dV}\right|_{\mathbf{r},V} \propto e^{-\frac{-z_s(\mathbf{r}}{z_0}} n(\mathbf{r}, E = eV) \propto \frac{n(\mathbf{r}, E = eV)}{\int_0^{eV_s} n(\mathbf{r}, E) \mathrm{d}E} \tag{S10}$$

This is the setup effect in which spatial variations in the density-of-electronic-states $n(\mathbf{r}, E)$ integrated to the "setup voltage" V_s yields a different proportionality between $\left.\frac{dI}{dV}\right|_{\mathbf{r},V}$ and $n(\mathbf{r}, E = eV)$ at different $\mathbf{r}$ (*55*).

The above demonstrates that the setup effect may give rise to spatial modulations in $\left.\frac{dI}{dV}\right|_{\mathbf{r},V}$ arising from both $n(\mathbf{r}, E = eV)$ and $\int_0^{eV_s} n(\mathbf{r}, E) \mathrm{d}E$. This does not, however, introduce modulations at wavevectors that are not already present in $n(\mathbf{r}, E)$. The novel signatures of field-induced PDW within the vortex halo reported in the main text are modulations with wavevector $\mathbf{Q} \cong (1/8, 0); (0, 1/8)\frac{2\pi}{a_0}$. The setup effect cannot artificially create these modulations and does not affect the conclusion of the main text.

6. Form Factor of $n(\mathbf{r}, E)$ Modulations resulting from PDW

In the main text we report the observation of a PDW through its attendant $n(\mathbf{r}, E)$ modulations.The $n(\mathbf{r}, E)$ modulations attendant to a PDW of wave-vector $\mathbf{Q_P}$, induced at a superconducting vortex, are that at wave-vector $\mathbf{Q}_P$ due to the product of PDW and uniform SC order parameters:

$$A_{Q_{\mathbf{Q_P}}} \propto \Delta_P^Q \Delta_{SC}^* \tag{S11}$$

and that at wave-vector $2\mathbf{Q_P}$ due to the product of the PDW order parameter with itself:

$$A_{2Q_{\mathbf{Q_P}}} \propto \Delta_P^Q \Delta_P^{-Q*} \ . \tag{S12}$$

The form factors of Δ_P^Q, $A_{Q_{\mathbf{Q_P}}}$ and $A_{2Q_{\mathbf{Q_P}}}$ are not true symmetry labels because the wavevector of the PDW does not transform into itself under any non-trivial element of the point group. Thus, eqns. S11 and S12 cannot formally be used to determine the form factor of the $n(\mathbf{r}, E)$ modulations from that of the PDW or vise versa. Generally, modulations of both form factor will be present.

However, as noted in reference (*43*), the form factor of these modulations may act approximately as symmetries due to the relatively long wavelength of the PDW modulations ($\approx 8a_0$). To the extent that this approximation is valid it implies that a d-wave superconductor coexisting in the vortex halo with a d-symmetry form factor PDW will give rise to s-symmetry form factor $n(\mathbf{r}, E)$ modulations at $\mathbf{Q_P}$ and $2\mathbf{Q_P}$. While recent microscopic calculations reported in reference (*43*) suggest that this approximate symmetry is indeed a valid description, this issue remains to be fully resolved (*22*).

7. Energy Dependence of $\delta g(\mathbf{r}, E)$

In figures S7 A-D we show $\delta g(\mathbf{r}, E)$ for $E = +30, +10, -10, -30$meV respectively. Each clearly shows magnetic field induced changes in the density of states at spatially isolated sites corresponding to superconducting vortices.

8. Measuring Gap Modulations

To detect the field induced gap modulations reported in figure 5E of the main text one needs to measure the gap as a function of position for both $B = 0$T and $B = 8.25$T. For each position $\mathbf{r}_i$ in a given differential conductance map we estimate the gap as follows:

- Find the E_i that has the maximal value of $g(\mathbf{r}_i, E_i, B)$ for $E > 0$ and denote this E_Δ.
- Fit a quadratic function to the set of the points $\{E_{\Delta-1}$,E_Δ,$E_{\Delta+1}\}$ and let the value of E at which these functions are maximal be denoted $\Delta(\mathbf{r}_i, B)$.

The field induced gap modulations are the revealed by calculating $\widetilde{\delta\Delta}(\mathbf{q}) = \mathrm{FT}\{\Delta(\mathbf{r}_i, B = 8.25\mathrm{T}) - \Delta(\mathbf{r}_i, B = 0\mathrm{T})\}$ (where FT denotes the Fourier transform) as shown in figure 5E of the main text.

9. Bidirectional vs. Unidirectional PDW

In the main text we show evidence that in $Bi_2Sr_2CaCu_2O_8$ a magnetic field induces an $8a_0$ period PDW with approximately equal amplitude along both $\mathbf{Q_x}$ and $\mathbf{Q_y}$ when averaged over the entire field of view. If there is no long range spatial phase coherence between the PDW halos induced at each vortex, this phenomenology can arise from two scenarios.

In the first scenario, each vortex halo contains a unidirectional PDW of the form

$$\Delta_{PD}(\mathbf{r}_1, \mathbf{r}_2) = D(\mathbf{r}_1 - \mathbf{r}_2) \left[\Delta_P^{\mathbf{Q}} e^{i\mathbf{Q}\cdot\mathbf{r}} + \Delta_P^{-\mathbf{Q}} e^{-i\mathbf{Q}\cdot\mathbf{r}} \right] \tag{S13}$$

where $\mathbf{Q}$ is either $\mathbf{Q_x}$ or $\mathbf{Q_y}$, with equal numbers of vortices choosing each of these wave-vectors. In the second scenario each vortex halo contains a bidirectional PDW of the form

$$\Delta_{PD}(\mathbf{r}_1, \mathbf{r}_2) = D(\mathbf{r}_1 - \mathbf{r}_2) \left[\Delta_{\mathbf{Q_x}} e^{i\mathbf{Q_x}\cdot\mathbf{r}} + \Delta_{\mathbf{Q_x}}^* e^{-i\mathbf{Q_x}\cdot\mathbf{r}} + \Delta_{\mathbf{Q_y}} e^{i\mathbf{Q_y}\cdot\mathbf{r}} + \Delta_{\mathbf{Q_y}}^* e^{-i\mathbf{Q_y}\cdot\mathbf{r}} \right] \tag{S14}$$

To distinguish between these scenarios we must establish whether the modulations along $\mathbf{Q_x}$ and $\mathbf{Q_y}$ coexist in each vortex halo or are spatially exclusive. To this end we can calculate the function

$$F(\mathbf{r}) = \frac{A_{\mathbf{Q_x}}(\mathbf{r}) - A_{\mathbf{Q_y}}(\mathbf{r})}{A_{\mathbf{Q_x}}(\mathbf{r}) + A_{\mathbf{Q_y}}(\mathbf{r})} \tag{S15}$$

where $A_{\mathbf{Q_x}}(\mathbf{r})$ is the local amplitude of $n(\mathbf{r}, E)$ modulations at wavevector $\mathbf{Q}$, as determined using the procedure given in reference (*45*). This function measures the local imbalance in amplitude along $\mathbf{Q_x}$ and $\mathbf{Q_x}$. Note that equ. S15 is invariant under transformations of the phases of modulations at $\mathbf{Q_x}$ and $\mathbf{Q_y}$ and thus is not affected by spatial variations in these phases.

In the case of a bidirectional PDW the distribution of F values in the vortex halos should be centered on $F = 0$ with a standard deviation much less than 1. In the case of a unidirectional PDW which randomly picks one of two directions in each halo the distribution should have significant weight near $|F| = 1$.

In figure S8 A we show $g(\mathbf{r}, +30\text{meV})$ masked so as to only show a 10nm region around the center of the eight most positionally stable vortices. These vortices were chosen because their vortex halo modulations exhibit minimal streaking which indicates that they were positionally stable. We exclude those vortices which moved significantly during measurement to avoid this motion corrupting our measurment of the modulation directionality. In figure S8 B we show the corresponding map of $F(\mathbf{r})$ derived from A. Note that only the eight most positionally stable vortices of 14 total vortices have been included in this masking function. While each vortex does show some amplitude imbalance in favor of one $\mathbf{Q_x}$ or $\mathbf{Q_y}$, this imbalance is small, indicating that $\mathbf{Q_x}$ and $\mathbf{Q_y}$ modulations coexist within each vortex halo. In figure S8 C we show the histogram of F values from all pixels within 10nm of a vortex center. This shows distribution of F values centered on $F = 0$ with a standard deviation of 0.08. While it has been shown that in the presence of disorder it is difficult to distinguish unidirectional and bidirectional density wave states in $g(\mathbf{r}, E)$ (*56*), the distribution in figure in figure S8 C is most consistent with a bidirectional state.

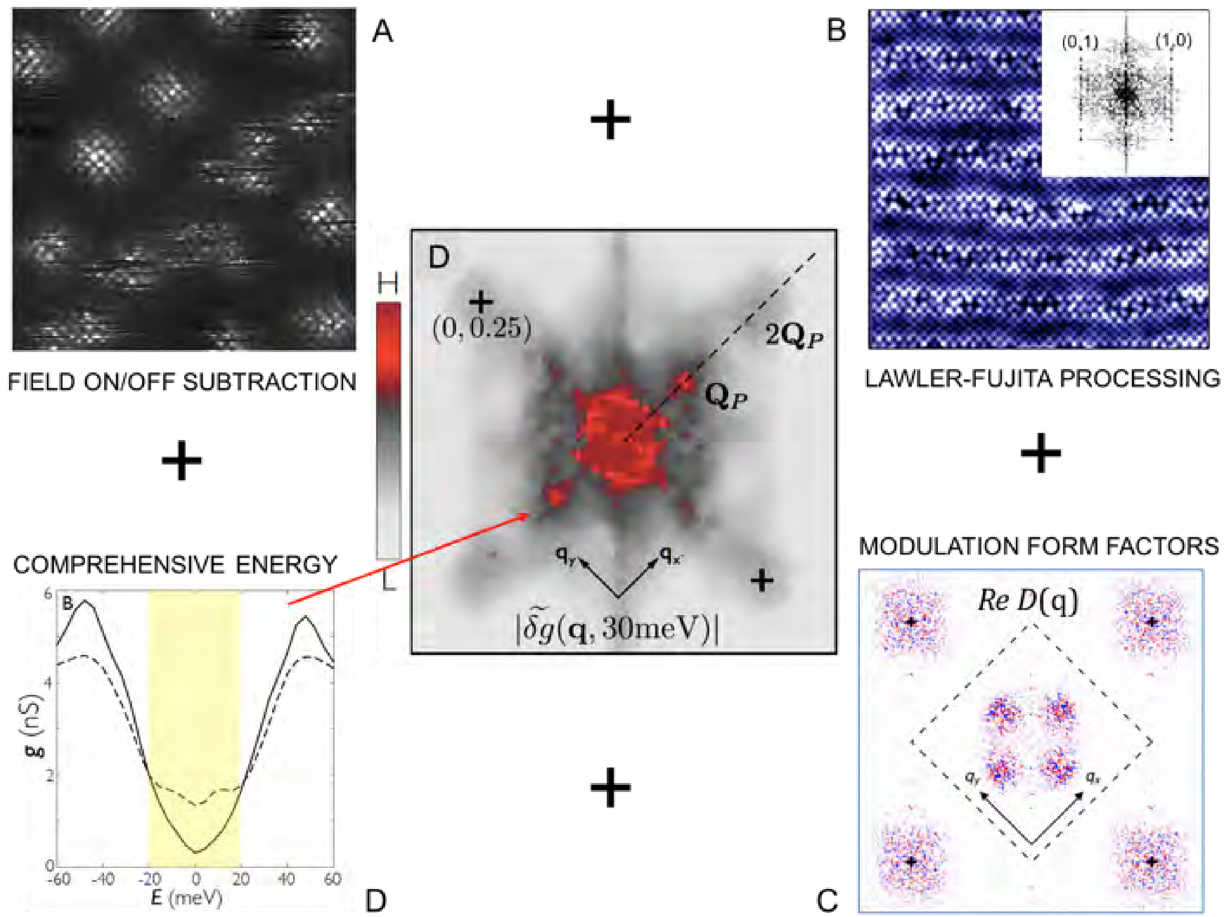

Figure S 1: (**A**) We study $\delta g(\mathbf{r}, E, B)$, the field induced perturbation to the electronic density of states in $Bi_2Sr_2CaCu_2O_8$. (**B**) All data are processes using the Lawler-Fujita algorithm rendering topographs $T(\mathbf{r}, V)$ and differential conductance maps $g(\mathbf{r}, E, B)$ distortion free and identically periodic. (**C**) Again, using Lawler-Fujita, the data is sublattice-phase-resolved so that the structure factor of all modulations is measured directly. **(D)**. The resulting field induced electronic structure changes $\delta g(\mathbf{r}, E, B)$ are measured in a wide range of energies from the node to beyond the gap edge. (**E**). Summary: studies in a larger FOV with higher vortex numbers (A), measured with sublattice-resolved spatial resolution (B,C), rendered distortion free and identically periodic (B), over a wide energy range (D), result in a far clearer and more precise picture of the electronic structure of the state within the cuprate vortex halo than has previously been reported.

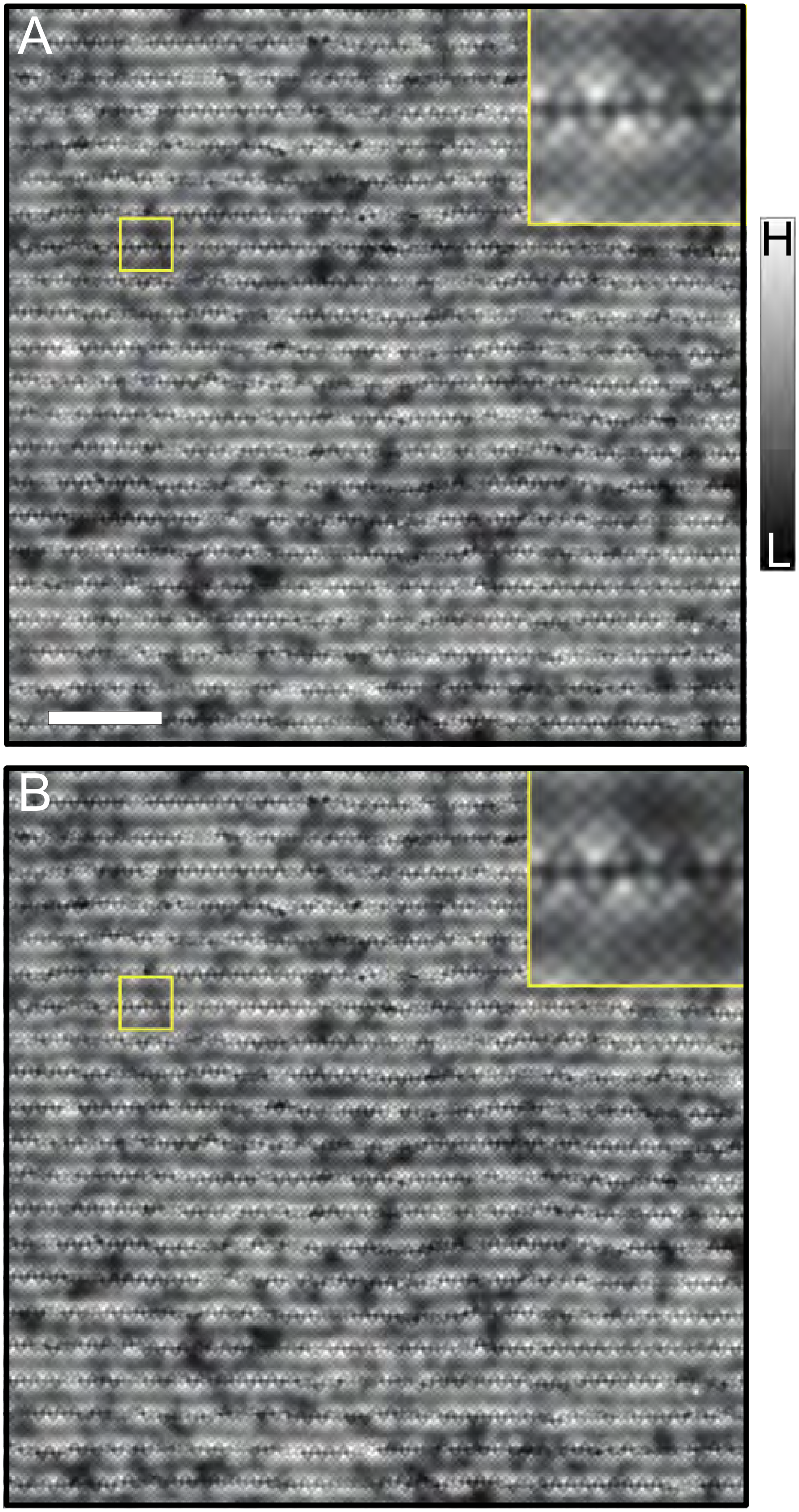

Figure S 2: Spatially registered topographs of $Bi_2Sr_2CaCu_2O_{8+\delta}$ taken at **(A)** $B = 8.25T$ and **(B)** $B = 0T$. The images show a 65nm × 65nm region of the sample and are registered to within 30 pm. Insets show magnified images of the region indicated by the yellow squares. The scale bar is 10nm long.

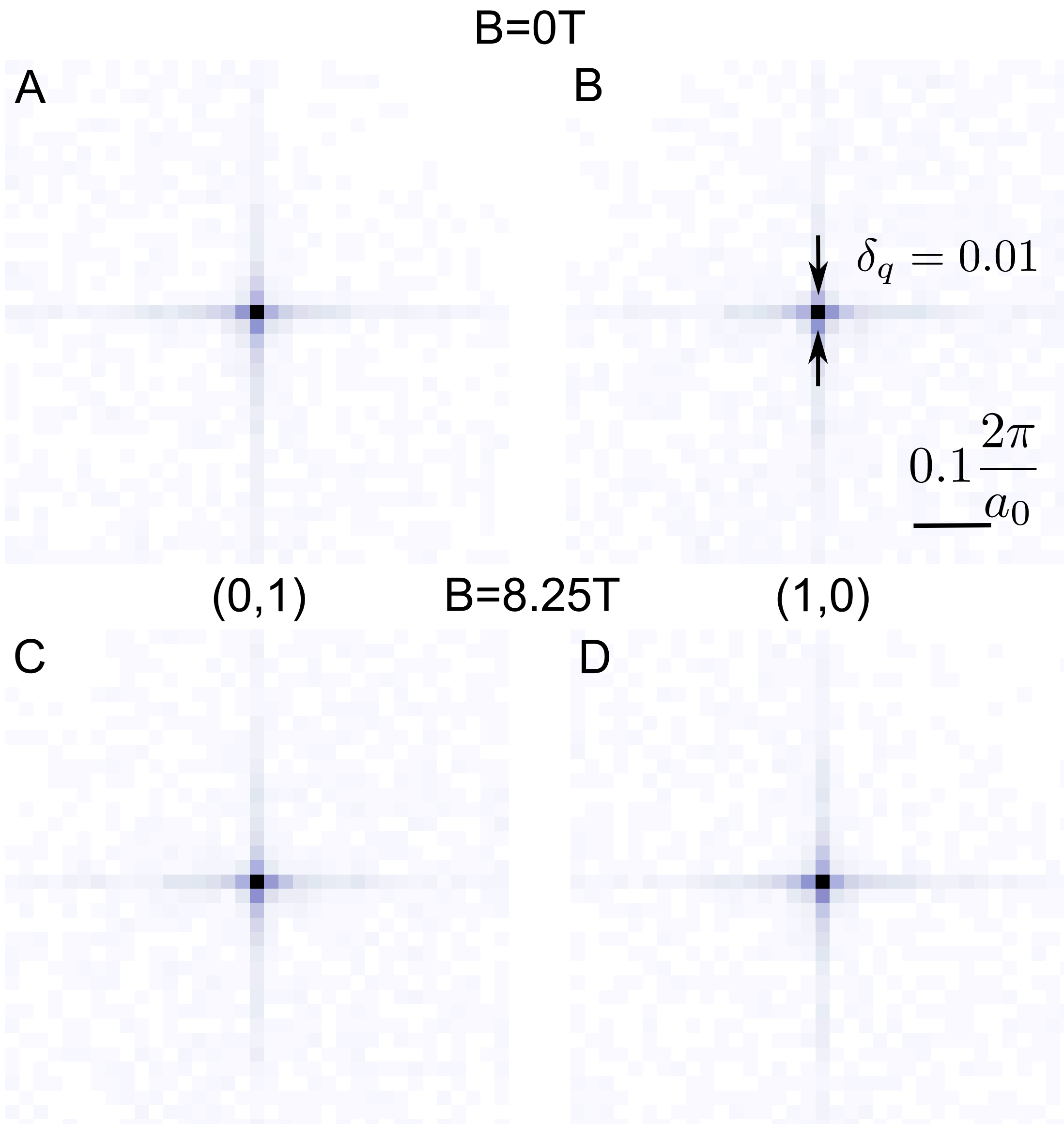

Figure S 3: Bragg peaks in Fourier transforms of topographs, $\tilde{T}(\mathbf{q})$, acquired simultaneously with spectroscopic data presented in figure 3E of the main text. **A** $\mathbf{q} = (0,1)\frac{2\pi}{a_0}$ Bragg peak in $\tilde{T}(\mathbf{q}, B = 0\text{T})$ **B** $\mathbf{q} = (1,0)\frac{2\pi}{a_0}$ Bragg peak in $\tilde{T}(\mathbf{q}, B = 0\text{T})$. The red circle shows the full-width at half-maximum of the Bragg peak δ_q. The scale bar is $0.1\frac{2\pi}{a_0}$ long. **C** $\mathbf{q} = (0,1)\frac{2\pi}{a_0}$ Bragg peak in $\tilde{T}(\mathbf{q}, B = 8.25\text{T})$ **D** $\mathbf{q} = (1,0)\frac{2\pi}{a_0}$ Bragg peak in $\tilde{T}(\mathbf{q}, B = 8.25\text{T})$

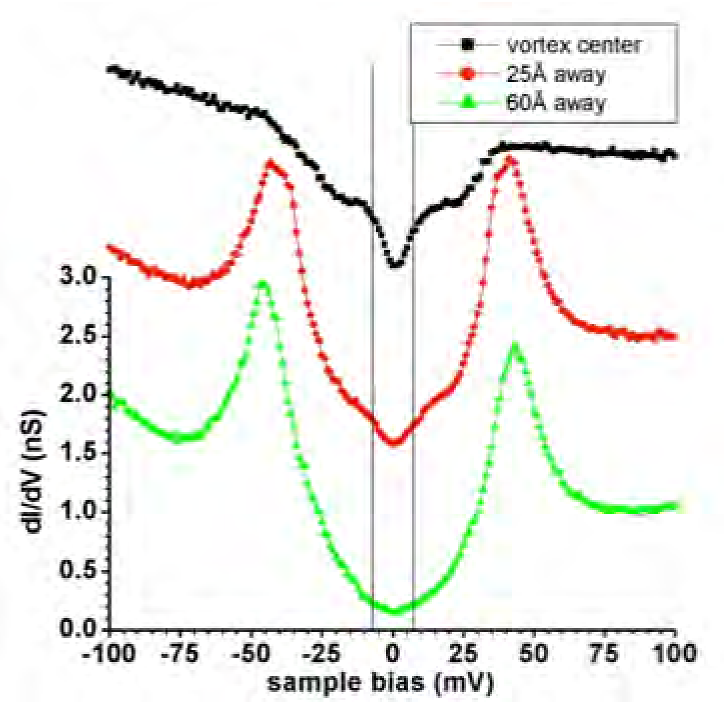

Figure S 4: $\frac{dI}{dV}$ spectra versus radial distance from the symmetry point of the $Bi_2Sr_2CaCu_2O_8$ vortex core.

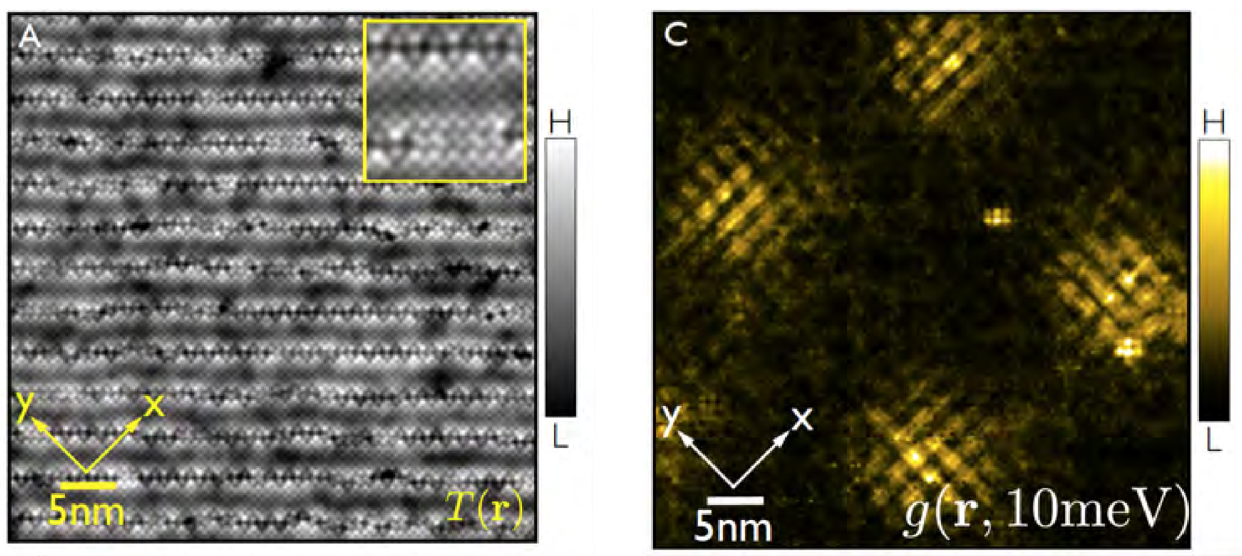

Figure S 5:
(**A**) Topographic image of FOV studied in B. (**B**). Differential conductance $g(\mathbf{r}, E)$ map at $E = 10$meV showing the Bogoliubov quasiparticle modulations within four vortex halos.

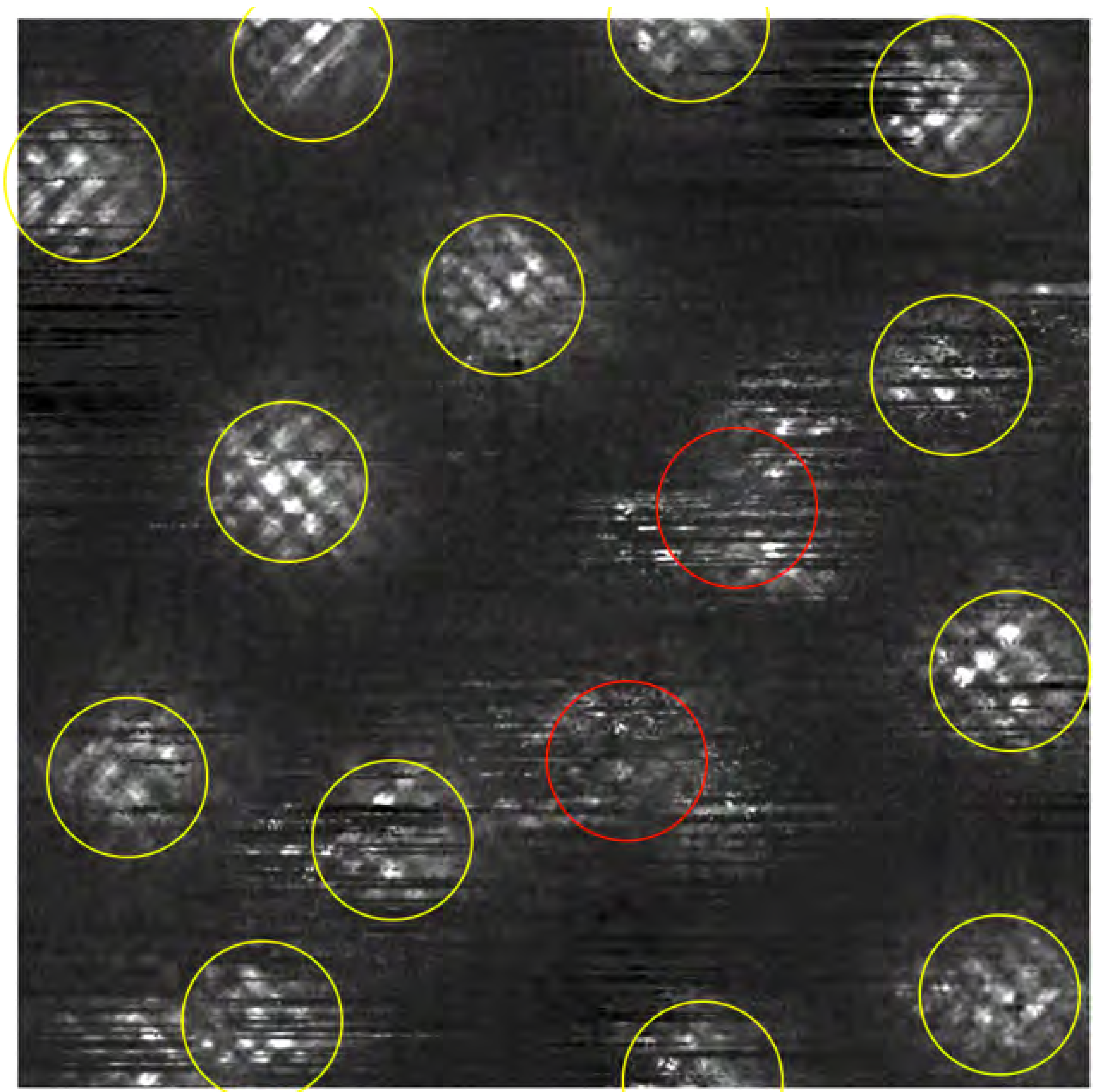

Figure S 6: A 58nm square FOV at B=8.25T should contain on the average fourteen $\phi = \frac{h}{2e}$ vortices. We observe 12 stable vortices clearly (yellow circles) and two regions of field induced electronic structure modulations (red circles) whose vortex halos were moving during the measurements

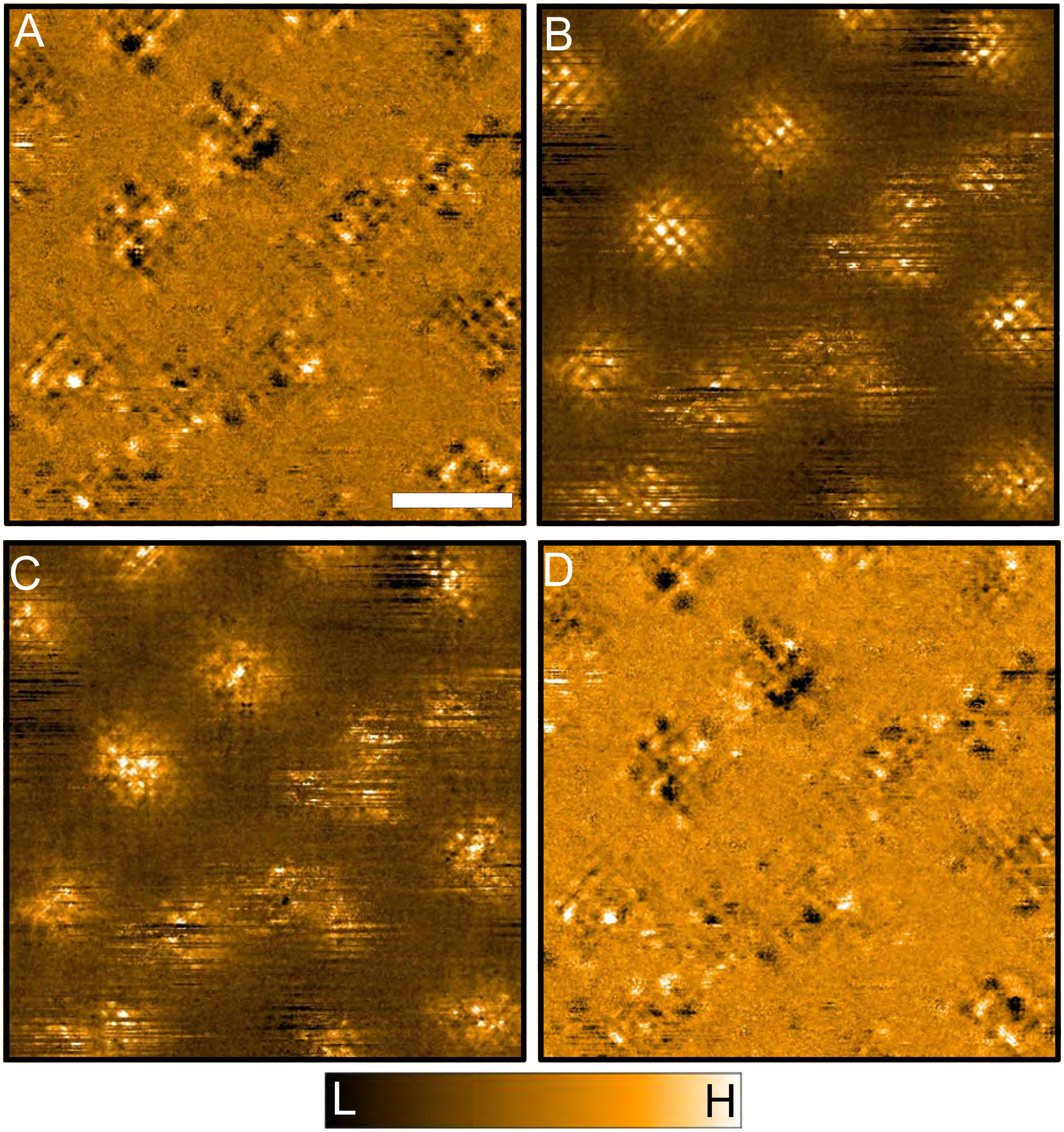

Figure S 7: $\delta g(\mathbf{r}, E)$ maps for the field of view analyzed in the main text at **(A)** $E = +30$meV **(B)** $E = +10$meV **(C)** $E = -10$meV **(D)** $E = -30$meV. The scale bar is 15nm long.

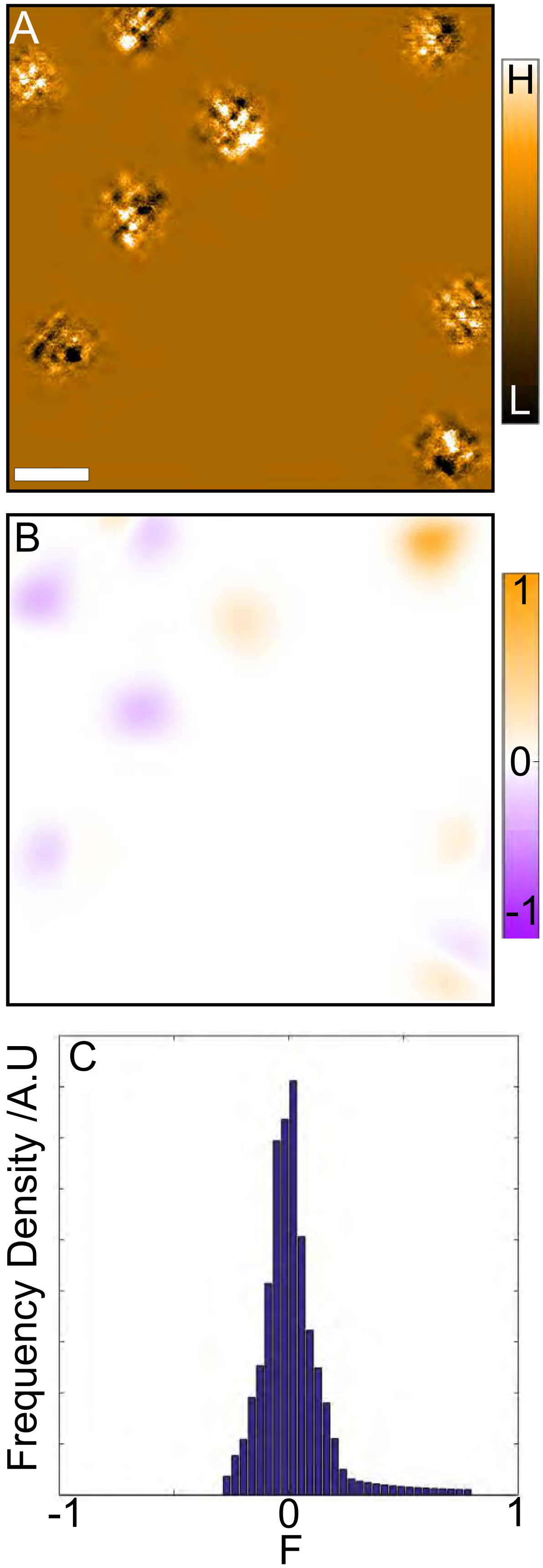

Figure S 8: **(A)** $g(\mathbf{r}, +30\text{meV})$ masked so as to only show a 10nm region around the center of each vortex. The scale bar is 10nm in length. **(B)** $F(\mathbf{r})$ derived from **A**. **(C)** Histogram of F values at all pixels within 10nm of vortex center.

References and Notes

1. P. Fulde, R. A. Ferrell, Superconductivity in a Strong Spin-Exchange Field. *Physical Review* **135**, A550–A563 (1964).
2. A. I. Larkin, Y. N. Ovchinnikov, Inhomogeneous state of superconductors. *Sov. Phys. JETP* **20**, 762–769 (1964).
3. E. Berg, E. Fradkin, E. A. Kim, S. A. Kivelson, V. Oganesyan, J. M. Tranquada, S. C. Zhang, Dynamical layer decoupling in a stripe-ordered high-T_c superconductor. *Physical Review Letters* **99**, 127003 (2007).
4. P. A. Lee, Amperean pairing and the pseudogap phase of cuprate superconductors. *Physical Review X* **4**, 1–13 (2014).
5. D. F. Agterberg, J. Garaud, Checkerboard order in vortex cores from pair-density-wave superconductivity. *Physical Review B* **104512** (2015).
6. A. Himeda, T. Kato, M. Ogata, Stripe states with spatially oscillating d-wave superconductivity in the two-dimensional t-t'-J model. *Physical Review Letters* **88**, 117001 (2002).
7. M. Raczkowski, M. Capello, D. Poilblanc, R. Frésard, A. M. Ole ś, Unidirectional d-wave superconducting domains in the two-dimensional $t-J$ model. *Physical Review B* **76**, 140505 (2007).
8. K.-Y. Yang, W. Q. Chen, T. M. Rice, M. Sigrist, F.-C. Zhang, Nature of stripes in the generalized t-J model applied to the cuprate superconductors. *New Journal of Physics* **11**, 055053 (2009).
9. F. Loder, A. P. Kampf, T. Kopp, Superconducting state with a finite-momentum pairing mechanism in zero external magnetic field. *Physical Review B* **81**, 020511(R) (2010).
10. P. Corboz, T. M. Rice, M. Troyer, Competing states in the t-J model: Uniform d-wave state versus stripe state. *Physical Review Letters* **113**, 046402 (2014).
11. R.-G. Cai, L. Li, Y.-Q. Wang, J. Zaanen, Intertwined Order and Holography: The Case of Parity Breaking Pair Density Waves. *Phys. Rev. Lett.* **119**, 181601 (2017).
12. Q. Li, M. Hücker, G. D. Gu, A. M. Tsvelik, J. M. Tranquada, Two-dimensional superconducting fluctuations in stripe-ordered $La_{1.875}Ba_{0.125}CuO_4$. *Physical Review Letters* **99**, 067001 (2007).
13. E. Berg, E. Fradkin, S. A. Kivelson, Charge-4e superconductivity from pair density wave order in certain high temperature superconductors. *Nature Physics* **5**, 830–833 (2009).
14. E. Berg, E. Fradkin, S. A. Kivelson, J. M. Tranquada, Striped superconductors: how spin, charge and superconducting orders intertwine in the cuprates. *New Journal of Physics* **11**, 115004 (2009).
15. C. Pépin, V. S. De Carvalho, T. Kloss, X. Montiel, Pseudogap, charge order, and pairing density wave at the hot spots in cuprate superconductors. *Physical Review B* **90**, 195207 (2014).
16. H. Freire, V. S. de Carvalho, C. Pépin, Renormalization group analysis of the pair-density-wave and charge order within the fermionic hot-spot model for cuprate superconductors. *Physical Review B* **92**, 045132 (2015).
17. Y. Wang, D. F. Agterberg, A. Chubukov, Coexistence of charge-density-wave and pair-density-wave orders in underdoped cuprates. *Physical Review Letters* **114**, 197001 (2015).
18. D. F. Agterberg, D. S. Melchert, M. K. Kashyap, Emergent loop current order from pair density wave superconductivity. *Phys. Rev. B* **91**, 054502 (2015).
19. M. Zelli, C. Kallin, A. J. Berlinsky, Mixed state of a π-striped superconductor. *Phys. Rev. B* **84**, 174525 (2011).
20. M. Zelli, C. Kallin, A. J. Berlinsky, Quantum oscillations in a π-striped superconductor. *Physical Review B* **86**, 104507 (2012).
21. M. R. Norman, J. C. S. Davis, Quantum oscillations in a biaxial pair density wave state. *Proceedings of the National Academy of Sciences* **115**, 5389–5391 (2018).
22. Z. Dai, Y.-H. Zhang, T. Senthil, P. A. Lee, Pair-density waves, charge-density waves, and vortices in high-T_c cuprates. *Phys. Rev. B* **97**, 174511 (2018).

23. F. Yu, M. Hirschberger, T. Loew, G. Li, B. J. Lawson, T. Asaba, J. B. Kemper, T. Liang, J. Porras, G. S. Boebinger, J. Singleton, B. Keimer, L. Li, N. P. Ong, Magnetic phase diagram of underdoped $YBa_2Cu_3O_y$ inferred from torque magnetization and thermal conductivity. *Proceedings of the National Academy of Sciences* **113**, 12667–12672 (2016).

24. M. H. Hamidian, S. D. Edkins, S. H. Joo, A. Kostin, H. Eisaki, S. Uchida, M. J. Lawler, E.-A. Kim, A. P. Mackenzie, K. Fujita, J. Lee, J. C. S. Davis, Detection of a Cooper-pair density wave in $Bi_2Sr_2CaCu_2O_{8+x}$. *Nature* **532**, 343–347 (2016).

25. T. Wu, H. Mayaffre, S. Krämer, M. Horvatić, C. Berthier, W. N. Hardy, R. Liang, D. a. Bonn, M.-H. Julien, Magnetic-field-induced charge-stripe order in the high-temperature superconductor $YBa_2Cu_3O_y$. *Nature* **477**, 191–194 (2011).

26. J. Chang, E. Blackburn, A. T. Holmes, N. B. Christensen, J. Larsen, J. Mesot, R. Liang, D. A. Bonn, W. N. Hardy, A. Watenphul, M. Zimmermann, E. M. Forgan, S. M. Hayden, Direct observation of competition between superconductivity and charge density wave order in $YBa_2Cu_3O_y$. *Nature Physics* **8**, 871–876 (2012).

27. D. LeBoeuf, S. Krämer, W. N. Hardy, R. Liang, D. a. Bonn, C. Proust, Thermodynamic phase diagram of static charge order in underdoped $YBa_2Cu_3O_y$. *Nature Physics* **9**, 79–83 (2012).

28. S. Blanco-Canosa, A. Frano, T. Loew, Y. Lu, J. Porras, G. Ghiringhelli, M. Minola, C. Mazzoli, L. Braicovich, E. Schierle, E. Weschke, M. Le Tacon, B. Keimer, Momentum-dependent charge correlations in $YBa_2Cu_3O_{6+\delta}$ superconductors probed by resonant x-ray scattering: Evidence for three competing phases. *Physical Review Letters* **110**, 187001 (2013).

29. T. Wu, H. Mayaffre, S. Krämer, M. Horvatić, C. Berthier, W. Hardy, R. Liang, D. Bonn, M.-H. Julien, Incipient charge order observed by NMR in the normal state of $YBa_2Cu_3O_y$. *Nature Communications* **6**, 6438 (2015).

30. S. Gerber, H. Jang, H. Nojiri, S. Matsuzawa, H. Yasumura, D. A. Bonn, R. Liang, W. N. Hardy, Z. Islam, A. Mehta, S. Song, M. Sikorski, D. Stefanescu, Y. Feng, S. A. Kivelson, T. P. Devereaux, Z.-X. Shen, C.-C. Kao, W.-S. Lee, D. Zhu, J.-S. Lee, Three-dimensional charge density wave order in $YBa_2Cu_3O_{6.67}$ at high magnetic fields. *Science* **350**, 949–952 (2015).

31. J. Chang, E. Blackburn, O. Ivashko, a. T. Holmes, N. B. Christensen, M. Hücker, R. Liang, D. a. Bonn, W. N. Hardy, U. Rütt, M. V. Zimmermann, E. M. Forgan, S. M. Hayden, Magnetic field controlled charge density wave coupling in underdoped $YBa_2Cu_3O_{6+x}$. *Nature Communications* **7**, 11494 (2016).

32. H. Jang, W.-S. Lee, H. Nojiri, S. Matsuzawa, H. Yasumura, L. Nie, A. V. Maharaj, S. Gerber, Y.-J. Liu, A. Mehta, D. A. Bonn, R. Liang, W. N. Hardy, C. A. Burns, Z. Islam, S. Song, J. Hastings, T. P. Devereaux, Z.-X. Shen, S. A. Kivelson, C.-C. Kao, D. Zhu, J.-S. Lee, Ideal charge-density-wave order in the high-field state of superconducting YBCO. *Proceedings of the National Academy of Sciences* **113**, 14645–14650 (2016).

33. B. Vignolle, D. Vignolles, M.-H. Julien, C. Proust, From quantum oscillations to charge order in high-copper oxides in high magnetic fields. *Comptes Rendus Physique* **14**, 39–52 (2013).

34. S. E. Sebastian, C. Proust, Quantum oscillations in hole-doped cuprates. *Annual Review of Condensed Matter Physics* **6**, 411–430 (2015).

35. J. E. Hoffman, E. W. Hudson, K. M. Lang, V. Madhavan, H. Eisaki, S. Uchida, J. C. Davis, A four unit cell periodic pattern of quasi-particle states surrounding vortex cores in $Bi_2Sr_2CaCu_2O_{8+\delta}$. *Science* **295**, 466–469 (2002).

36. K. Matsuba, S. Yoshizawa, Y. Mochizuki, T. Mochiku, K. Hirata, N. Nishida, Anti-phase Modulation of Electron- and Hole-like States in Vortex Core of $Bi_2Sr_2CaCu_2O_x$ Probed by Scanning Tunneling Spectroscopy. *Journal of the Physical Society of Japan* **76**, 063704 (2007).

37. S. Yoshizawa, T. Koseki, K. Matsuba, T. Mochiku, K. Hirata, N. Nishida, High-Resolution Scanning Tunneling Spectroscopy of Vortex Cores in Inhomogeneous Electronic States of $Bi_2Sr_2CaCu_2O_x$. *Journal of the Physical Society of Japan* **82**, 083706 (2013).

38. T. Machida, Y. Kohsaka, K. Matsuoka, K. Iwaya, T. Hanaguri, T. Tamegai, Bipartite electronic superstructures in the vortex core of $Bi_2Sr_2CaCu_2O_{8+\delta}$. *Nature Communications* **7**, 11747 (2016).

39. S. A. Kivelson, D.-h. Lee, E. Fradkin, V. Oganesyan, Competing order in the mixed state of high-temperature superconductors. *Physical Review B* **66**, 144516 (2002).

40. D. F. Agterberg, H. Tsunetsugu, Dislocations and vortices in pair density wave superconductors. *Nature Physics* **4**, 639–642 (2009).

41. J. D. Sau, S. Sachdev, Mean-field theory of competing orders in metals with antiferromagnetic exchange interactions. *Phys. Rev. B* **89**, 075129 (2014).

42. M. Einenkel, H. Meier, C. Pépin, K. B. Efetov, Vortices and charge order in high-T_c superconductors. *Phys. Rev. B* **90**, 054511 (2014).

43. Y. Wang, S. D. Edkins, M. H. Hamidian, J. C. S. Davis, E. Fradkin, S. A. Kivelson, Pair density waves in superconducting vortex halos. *Phys. Rev. B* **97**, 174510 (2018).

44. Materials and methods are available as supplementary materials.

45. M. H. Hamidian, S. D. Edkins, C. K. Kim, J. C. Davis, A. P. Mackenzie, H. Eisaki, S. Uchida, M. J. Lawler, E. A. Kim, S. Sachdev, K. Fujita, Atomic-scale electronic structure of the cuprate d-symmetry form factor density wave state. *Nature Physics* **12**, 150–156 (2016).

46. M. J. Lawler, K. Fujita, J. Lee, a. R. Schmidt, Y. Kohsaka, C. K. Kim, H. Eisaki, S. Uchida, J. C. Davis, J. P. Sethna, E.-A. Kim, Intra-unit-cell electronic nematicity of the high-T_c copper-oxide pseudogap states. *Nature* **466**, 347–351 (2010).

47. N. Schopohl, K. Maki, Quasiparticle spectrum around a vortex line in a d-wave superconductor. *Phys. Rev. B* **52**, 490–493 (1995).

48. M. Ichioka, N. Hayashi, N. Enomoto, K. Machida, Vortex structure in d-wave superconductors. *Phys. Rev. B* **53**, 15316–15326 (1996).

49. M. Franz, C. Kallin, P. I. Soininen, A. J. Berlinsky, A. L. Fetter, Vortex state in a d-wave superconductor. *Phys. Rev. B* **53**, 5795–5814 (1996).

50. Y. Morita, M. Kohmoto, K. Maki, Quasiparticle Spectra around a Single Vortex in a d-Wave Superconductor. *Phys. Rev. Lett.* **78**, 4841–4844 (1997).

51. M. Franz, Z. Tešanović, Self-consistent electronic structure of a $d_{x^2-y^2}$ and a $d_{x^2-y^2} + id_{xy}$ vortex. *Phys. Rev. Lett.* **80**, 4763–4766 (1998).

52. H. Nishimori, K. Uchiyama, S.-i. Kaneko, A. Tokura, H. Takeya, K. Hirata, N. Nishida, First Observation of the fourfold-symmetric and quantum regime vortex core in YNi_2B_2C by scanning tunneling microscopy and spectroscopy. *Journal of the Physics Society Japan* **73**, 3247–3250 (2004).

53. H. Sakata, M. Oosawa, K. Matsuba, N. Nishida, H. Takeya, K. Hirata, Imaging of a Vortex Lattice Transition in YNi_2B_2C by Scanning Tunneling Spectroscopy. *Physical Review Letters* **84**, 1583–1586 (2000).

54. T. Klein, I. Joumard, S. Blanchard, J. Marcus, R. Cubitt, T. Giamarchi, P. Le Doussal, A Bragg glass phase in the vortex lattice of a type II superconductor. *Nature* **413**, 404–406 (2001).

55. A. J. Macdonald, Y. S. Tremblay-Johnston, S. Grothe, S. Chi, P. Dosanjh, S. Johnston, S. A. Burke, Dispersing artifacts in FT-STS: A comparison of set point effects across acquisition modes. *Nanotechnology* **27**, 414004 (2016).

56. J. Robertson, S. Kivelson, E. Fradkin, A. Fang, A. Kapitulnik, Distinguishing patterns of charge order: Stripes or checkerboards. *Physical Review B* **74**, 134507 (2006).